NASA Technical Memorandum 83138

SPACE SHUTTLE ORBITER FLIGHT HEATING RATE MEASUREMENT SENSITIVITY TO THERMAL PROTECTION SYSTEM UNCERTAINTIES

Pamela F. Bradley and David A. Throckmorton

June 1981

National Aeronautics and Space Administration

Langley Research Center
Hampton, Virginia 23665

SPACE SHUTTLE ORBITER FLIGHT HEATING RATE MEASUREMENT SENSITIVITY TO THERMAL PROTECTION SYSTEM UNCERTAINTIES

Pamela F. Bradley
and
David A. Throckmorton

SUMMARY

A study has been completed to determine the sensitivity of computed convective heating rates to uncertainties in the Thermal Protection System (TPS) thermal model. Those parameters considered were: density, thermal conductivity, and specific heat of both the reusable surface insulation (RSI) and its coating, coating thickness and emittance, and temperature measurement uncertainty. The assessment used a modified version of the computer program described in NASA TM X-3370 to calculate heating rates from temperature-time histories. The original version of the program solves the "direct" one-dimensional heating problem and this modified version of the program is set up to solve the "inverse" problem. The modified program is intended for use in thermocouple data reduction for shuttle flight data. Both nominal thermal models and altered thermal models were used in the study to determine the necessity for accurate knowledge of the thermal protection system's material thermal properties. For many thermal properties the sensitivity (inaccuracies created in the calculation of convective heating rate by an altered property) is very low; however, a great dependence on the front surface reradiative term requires accurate knowledge of emissivity and surface temperature for an accurate heating rate determination.

INTRODUCTION

Development Flight Instrumentation (DFI) on the Space Shuttle Orbiter will provide engineers with an opportunity to conduct flight aerothermodynamic research using the Orbiter as a flight research vehicle. Definition of the heating environment experienced by the shuttle's thermal protection system throughout the entry trajectory is a significant part of this research. A large number of thermocouples (approximately 225) distributed about the Orbiter surface will provide for measurement of surface temperature-time histories during the entire entry trajectory. These temperature-time histories will be used in the calculation of convective heating rate, hence defining the Orbiter's entry heating environment.

Determination of the convective heating rate to the surface of the TPS requires an inverse solution to the transient, one-dimensional heat conduction problem (i.e., solve for heating rate given the surface temperature history). This solution is applied to a multi-layer, insulative TPS which is physically different at each measurement point on the vehicle. Therefore, an existing solution method was sought which had multi-layer capability and was computationally efficient, and which provided the required solution accuracy.

A search of various methods and available computer programs eliminated a number of possible methods (refs. 1 to 6) for various reasons. Some were too expensive computationally (refs. 1 to 3), while others were not specific to the multi-layer insulative system problem (refs. 3 to 6). The computer program described in NASA TM X-3370 (Pittman and Brinkley, ref. 7) was chosen for its low cost in computer time and its applicability to the shuttle's layered TPS. Although this program provides a solution to the "direct problem," a simple modification to the finite difference equation at the heated surface allows for specification of the surface temperature-time history and solution for the convective heating rate.

The accuracy of the calculated convective heating rate is dependent upon accurate knowledge of the location of the temperature measurement within the TPS, the thermal properties of the TPS materials, and the layer thicknesses. Using the Pittman and Brinkley program SINK in both the "direct" and "inverse" forms, the sensitivity of the calculated heating rate to uncertainties in thermal properties, layer thicknesses, and surface temperature has been determined.

SYMBOLS

C_p	specific heat, J/kg-K
C_s	heat capacity of front surface heat sink ($\rho C_p t$), J/m^2-K
h_e	total enthalpy at edge of boundary layer, J/kg
h_w	local enthalpy of fluid at front surface temperature, J/kg
k	thermal conductivity, W/m-K
q_{CALC}	q_c as calculated by the inverse method, W/m^2
q_{GIVEN}	q_c input to direct method, W/m^2
q_c	cold-wall convective heating rate, W/m^2
q_R	radiant heating rate to the surface, W/m^2
q_{RR}	reradiated heating rate ($\sigma \varepsilon_{s,1} T_1^4$), W/m^2
T	temperature, K
T_1	temperature of first station of layer, K

t	heat sink thicknesses, m
x	coordinate normal to surface
α	absorptance of front surface
$\varepsilon_{s,1}$	emittance of front surface
σ	Stefan-Boltzmann constant, $W/m^2\text{-}K^4$
τ	time, sec

ANALYSIS

Description of Method

The original version (ref. 7) of the SINK program provides a one-dimensional analysis of the transient thermal response of multi-layer insulative systems. The surface heating rate, initial temperature distribution through the material, and material properties and layer thicknesses must be specified for solution. The program can handle multiple layers of material and air gaps between layers and at the back surface. The program can have both radiative and convective heating rate inputs. Its most applicable feature to the inverse problem is that the temperature at any one station in the TPS material can be specified as a function time. With the front surface temperature specified (station 1), a simple modification to the front surface boundary condition allows calculation of convective heating rate. In finite difference form, the convective heating rates at the beginning and the end of each time step are assumed equal, as are the enthalpies. This assumption gives the result shown below in equation (1). (Terms are not shown differenced here.)

$$q_c = \frac{1}{(1-\frac{h_w}{h_e})}\left[-\alpha\, q_R - k\frac{\partial T}{\partial x} + \sigma\varepsilon_{s,1}\, T_1^{\,4} + C_s\frac{\partial T_1}{\partial \tau}\right]. \qquad (1)$$

For this calculation, q_R is assumed zero. This is the only modification to the SINK program.

Thermal Models

Three different thermal models were used in the conduct of this study. The models provide mathematical representations of each of the three TPS types present on the Orbiter. The TPS types and thermal models are described below, and in figures 1 to 3.

High-Temperature Reusable Surface Insulation (HRSI) - Figure 1

Consists of a Silica tile (with a high-emittance, black, water-proof coating) bonded to a felt strain isolator pad (SIP), which is in turn bonded to the vehicle structure.	Model:	
	Coating	4 Nodes
	Tile	86 Nodes
	Adhesive	2 Nodes
	SIP	2 Nodes
	Adhesive	2 Nodes
	Structure	2 Nodes

Low-Temperature Reusable Surface Insulation (LRSI) - Figure 2

Consists of a Silica tile (with a high-reflectance, white, water-proof coating) bonded to a felt SIP, which is in turn bonded to the vehicle structure.	Model:	
	Coating	4 Nodes
	Tile	86 Nodes
	Adhesive	2 Nodes
	SIP	2 Nodes
	Adhesive	2 Nodes
	Structure	4 Nodes

Flexible Reusable Surface Insulation (FRSI) - Figure 3

Consists of a blanket of felt (with a high-reflectance, white, water-proof coating) bonded to the vehicle structure.	Model:	
	Coating	4 Nodes
	Felt	86 Nodes
	Adhesive	6 Nodes
	Structure	4 Nodes

Layer thickness dimensions shown in figures 1 to 3 are applicable to the specific body points modeled for the purpose of this study. Body point locations are shown in figures 4 and 5. Heating rate and pressure information was for trajectory 14414.1C. The Appendix gives thermal property information used in this study.

Accuracy of Method

In order to assess the accuracy of the inverse solution technique, the direct solution was applied to known heating-rate histories for each of the selected body points to generate surface temperature-time histories, using nominal thermal models. These temperature-time histories were then used as input to the inverse solution, again with nominal thermal models, in order to generate computed heating rate histories. Comparison of the computed heating rate histories with the original given heating-rate histories provides a measure of the accuracy of the solution technique. This comparison is shown in figures 6 to 9 for two of the body points. Solution error is not significant for trajectory times between 100 and 1500 seconds for any of the body points studied.

Sensitivity Analysis

After the accuracy of the modified method was established, the method was used to parametrically determine the sensitivity of the calculated heating rate to uncertainties in thermal model parameters. The surface temperature-time histories generated using the direct solution with nominal thermal models were used as inputs to inverse solutions in which thermal model parameters were systematically varied.

The sensitivity of the solution to an uncertainty in a thermal model parameter appears as an error in the computed convective heating rate when compared to the input heating rate of the direct solution. Table I gives a list of the parameter variations considered in the study.

RESULTS AND DISCUSSION

Although all variations listed in Table I were investigated, most had an insignificant effect upon the computed result; therefore, only those found to be significant will be discussed. The calculated convective heating rate for the HRSI system is affected by uncertainties in the surface emittance and the surface temperature. A 5-percent uncertainty in the surface emittance creates a 5-percent error in the calculated convective heating rate. This is shown in figure 10. A 5-percent change in surface temperature (thermocouple error), figures 11 and 12, creates a 20-percent error in the convective heating rate calculation. The source of these errors is illustrated in figure 13 which shows a plot typical of the HRSI system with the convective heating rate and the reradiative term plotted versus time. The dominance of the reradiative term in the equation for q_c (eq. (1)) is evident from this plot. Consequently, a 5-percent change in emittance causes a 5-percent change in the reradiative term, and a 5-percent change in surface temperature is magnified by the fourth power in the reradiative term.

The LRSI and FRSI systems showed similar results (figs. 14 to 19) but additionally, significant errors in the calculated heating rate were noted from 0 to 400 seconds and from 1200 to 1600 seconds in the trajectory, when the coating thicknesses were doubled (figs. 20 and 21). However, in the high heating phase of the trajectory, errors in the coating thickness will create errors in the calculation of less than 5 percent. No other parameter variations significantly affect the convective heating-rate calculation.

A direct solution was obtained for the various RSI tile systems with temperature data from 0.076 cm (0.03 in) below the surface stored for use in the inverse calculations. These interior temperatures were used in the heating rate calculations as assumed surface temperatures to assess the errors resulting from a thermocouple which is not in thermal contact with the surface. The resulting errors in heating rate calculations are shown in figures 22 to 27. Results indicate that for similar types of tiles and similar depth of thermocouples, the solution gives similar error in heating rate for different heating environments.

This indicates that a correction might be applied to shuttle data based on type of tile and thermocouple depth for the various heating environments, if thermocouple depth is known.

An investigation to determine the effect of uncertainty in the initial temperature distribution through the material on the calculated heating rate was also completed. Both high and low backface temperatures were investigated with the temperature varying linearly through the material to the given surface temperature. A 55 K variation from front surface to back was imposed. The effect on the calculation for convective heating rate was insignificant.

CONCLUDING REMARKS

A study has been completed to determine the sensitivity of computed convective heating rates to uncertainties in the TPS thermal model. The assessment used a modified version of the SINK program described in NASA TM X-3370 to calculate heating rates from temperature-time histories. Both nominal thermal properties and altered thermal properties were used. The modified program is intended for use in thermocouple data reduction for shuttle flight data. The necessity for accurate knowledge of the thermal properties and layer thicknesses of the shuttle's thermal protection system was determined by the sensitivity study. Results of the study show very low sensitivity for many thermal properties; however, a great dependence on the front surface reradiative term was shown for accurate calculation of the convective heating rate. This dependence requires accurate knowledge of the surface emissivity and surface temperature for an accurate convective heating rate calculation. A slight dependence on the surface coating thickness was also determined for the LRSI and FRSI systems. Therefore, thermal properties of the shuttle's insulative system can vary from nominal properties (those specified by the manufacturer) somewhat without affecting the calculation of convective heating rate. However, due to the affect of the reradiative term in the calculation, accurate knowledge of the surface temperature and emissivity is desired for an accurate convective heating-rate calculation.

Appendix

Material Properties

HRSI Tiles

I. Coating

Thickness	3.81×10^{-4} m
Density	1666 kg/m^3
Emittance	0.85
Absorptance	0.85

Temperature (^{o}K)	Thermal Conductivity (W/m-K)	Specific Heat (J/kg-K)
255.6	0.843	794.96
533.3	1.045	1004.16
811.1	1.218	1192.44
1088.9	1.378	1317.96
1227.8	1.449	1360.72
1366.7	1.528	1443.48
1450.0	1.565	1476.95
1644.4	1.687	1569.00
1811.1	1.870	1631.76
1922.2	2.042	1631.76

II. LI-900 RSI

Thickness	7.94×10^{-2} m
Density	144.17 kg/m^3

Temperature (^{o}K)	Thermal Conductivity (W/m-K) Pressure (N/m^2)						Specific Heat (J/kg-K)
	0	10.05	100.5	1013.0	10131.0	101314.6	
255.6	0.0130	0.0130	0.0173	0.0317	0.0433	0.0476	627.6
394.4	0.0160	0.0160	0.0216	0.0390	0.0547	0.0600	878.64
533.3	0.0216	0.0216	0.0290	0.0478	0.0700	0.0750	1054.37
672.2	0.0303	0.0303	0.0374	0.0562	0.0850	0.0924	1150.60
811.0	0.0403	0.0403	0.0476	0.0680	0.1040	0.1140	1205.00
950.0	0.0533	0.0533	0.0606	0.0850	0.1255	0.1353	1238.46
1088.9	0.0720	0.0720	0.0800	0.1068	0.1514	0.1630	1255.20
1227.8	0.0980	0.0980	0.1056	0.1330	0.1835	0.1960	1263.57
1366.7	0.1270	0.1270	0.1353	0.1630	0.2200	0.2350	1267.75
1533.3	0.1670	0.1670	0.1765	0.2008	0.2700	0.2900	1267.75

III. RTV-560 (Room Temperature Vulcanizing)

Thickness	1.78×10^{-4} m
Density	1409.7 Kg/m^3
Thermal Conductivity	0.3115 W/m-K
Specific Heat	1464.40 J/kg-K

IV. SIP

Thickness 4.064×10^{-3} m
Density 86.5 kg/m^3

Temperature (°K)	Thermal Conductivity (W/m-K) Pressure (N/m^2)						Specific Heat (J/kg-K)
	0	10.05	100.5	1013.0	10131.0	101314.6	
255.6	0.0092	0.0092	0.0190	0.0308	0.0343	0.0355	794.96
311.1	0.0098	0.0098	0.0215	0.0360	0.0407	0.0422	1079.47
366.7	0.0109	0.0109	0.0234	0.0415	0.0472	0.0493	1439.30
422.2	0.0126	0.0126	0.0263	0.0471	0.0550	0.0571	1882.80
477.8	0.0157	0.0157	0.0291	0.0524	0.0642	0.0661	2405.80

V. RTV-560 (same as III)

VI. Aluminum 2219-T8XX

Thickness 6.35×10^{-3} m
Density 2803.4 kg/m^3

Temperature (°K)	Thermal Conductivity (W/m-K)	Specific Heat (K/kg-K)
255.6	119.42	
311.1	128.07	
366.7	135.00	899.56
422.2	141.92	928.85
477.8	146.60	953.95
533.3	150.57	979.06

LRSI Tiles

I. Coating

Thickness 3.05×10^{-6} m
Density 1666.0 kg/m^3
Emittance 0.80
Absorptance 0.32
Thermal Conductivity } same as HRSI Coating
Specific Heat }

II. LI-900 RSI

Thickness 0.014 m
All Thermal Properties same as HRSI

III. RTV-560 - same as HRSI RTV-560

IV. SIP - same as HRSI SIP

V. RTV-560 - same as HRSI RTV-560

VI. Aluminum 2219-T8XX - same as HRSI item VI

FRSI Tiles

I. Coating

Thickness	1.76×10^{-5} m
Density	1553.86 kg/m^3
Emittance	0.80
Absorptance	0.32
Thermal Conductivity	0.3115 W/m-K
Specific Heat	1464.4 J/kg-K

II. Felt

Thickness	4.064×10^{-3} m, 8.128×10^{-3} m
Density	86.5 kg/m^3

Temperature (°K)	Thermal Conductivity W/m-K Pressure (N/m^2)							Specific Heat (J/kg-K)
	0	1.005	10.05	100.5	1013.0	10131.0	101314.6	
255.6	0.0138	0.0138	0.0182	0.0242	0.0300	0.0343	0.0356	1305.41
311.1	0.0149	0.0149	0.0208	0.0287	0.035	0.0412	0.0433	-
366.7	0.0164	0.0164	0.0240	0.0336	0.0415	0.0476	0.0502	1388.90
422.2	0.0176	0.0176	0.0270	0.0384	0.0476	0.0560	0.0580	-
477.8	0.0190	0.0190	0.0294	0.0433	0.0547	0.0640	0.0665	1401.64
588.9	0.0225	0.0225	0.0360	0.0545	0.0704	0.0822	0.0846	1443.42
700.0	0.0260	0.0260	0.0433	0.0658	0.0865	0.1052	0.1073	1506.24
311.1	0.0303	0.0303	0.0520	0.0800	0.1064	0.1340	0.1376	1589.92

III. RTV-560 - same as HRSI RTV-560

IV. Aluminum 2219-T8XX - same as HRSI item VI

REFERENCES

1. Garrett, L. Bernard; and Pitts, Joan I.: A General Transient Heat-Transfer Computer Program for Thermally Thick Walls. NASA TM X-2058, 1970.

2. Anon: Martin Interactive Thermal Analysis System Version 2.0, Martin Marietta Corp. MDS-SPLPD-71-FD238 (Rev. 3).

3. Williams, S. D.; and Curry, D. M.: An Analytical and Experimental Study for Surface Heat Flux Determination. Journal of Spacecraft and Rockets, Vol. 14, Oct. 1977.

4. Stolz, G., Jr.: Numerical Solutions to an Inverse Problem of Heat Conduction for Simple Shapes. Journal of Heat Transfer, Vol. 82, No. 1, Feb. 1960.

5. Sparrow, E. M.; Haji-Sheikh, A.; and Lundgren, T. S.: The Inverse Problem in Transient Heat Conduction. Journal of Applied Mechanics, Vol. 31 Series E, No. 3, Sept. 1964.

6. Beck, James V.; and Wolf, Herbert: The Nonlinear Inverse Heat Conduction Problem. American Society of Mechanical Engineers and American Institute of Chemical Engineers, Heat Transfer Conference and Exhibit, Los Angeles, California. 65-HT-40, Aug. 1965.

7. Pittman, Claud M.; and Brinkley, Kay L.: One-Dimensional Numerical Analysis of the Transient Thermal Response of Multilayer Insulative Systems. NASA TM X-3370, 1976.

TABLE I.- THERMAL MODEL PARAMETER VARIATIONS CONSIDERED

Temperature	± 5%
RSI Density	± 30%
RSI Thermal Conductivity	± 30%
RSI Specific Heat	± 30%
Coating Thickness	±100%
Coating Density	± 30%
Coating Thermal Conductivity	± 30%
Coating Specific Heat	± 30%
Coating Emittance	± 5%

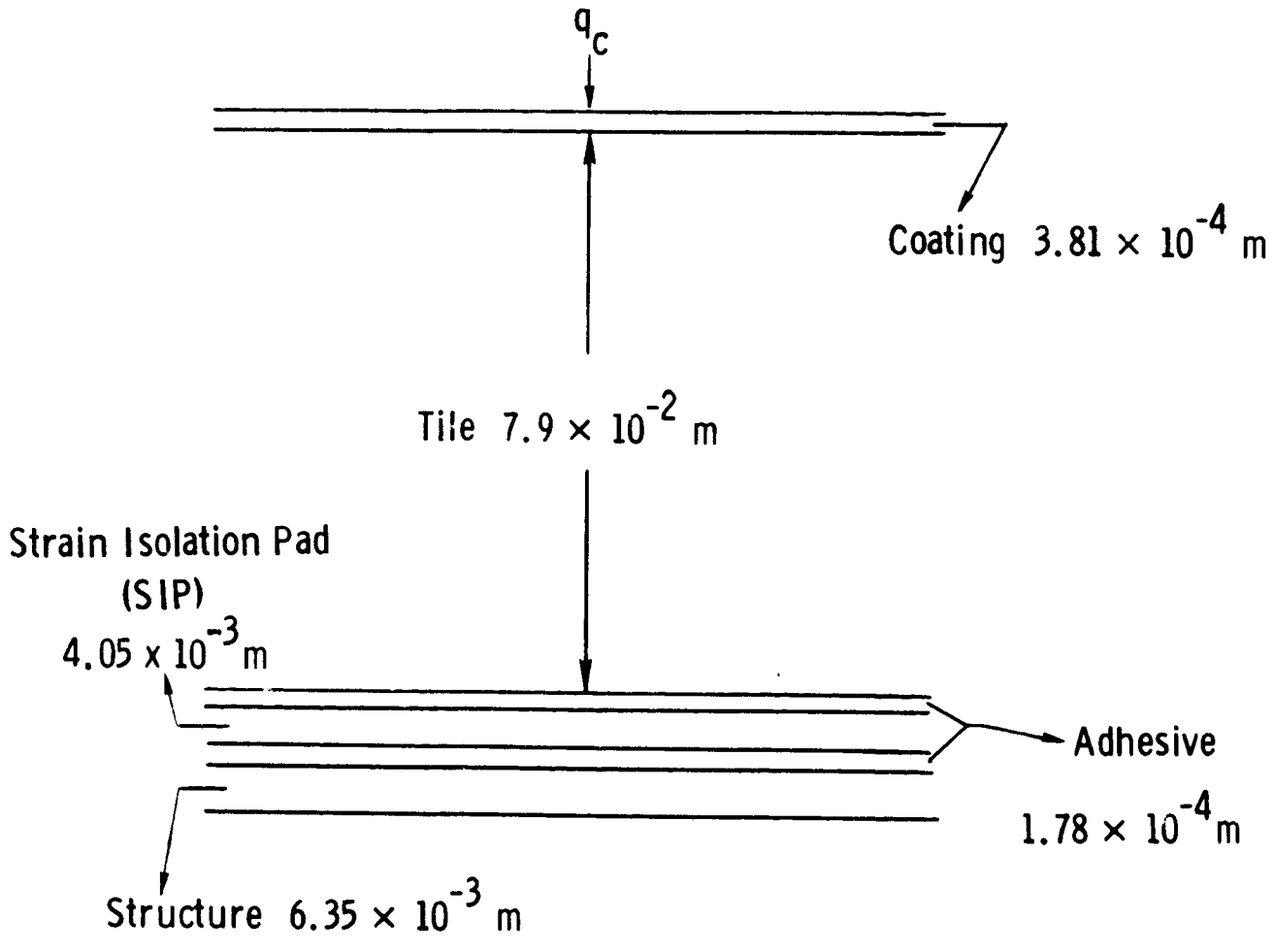

Figure 1.- HRSI thermal model (not drawn to scale).

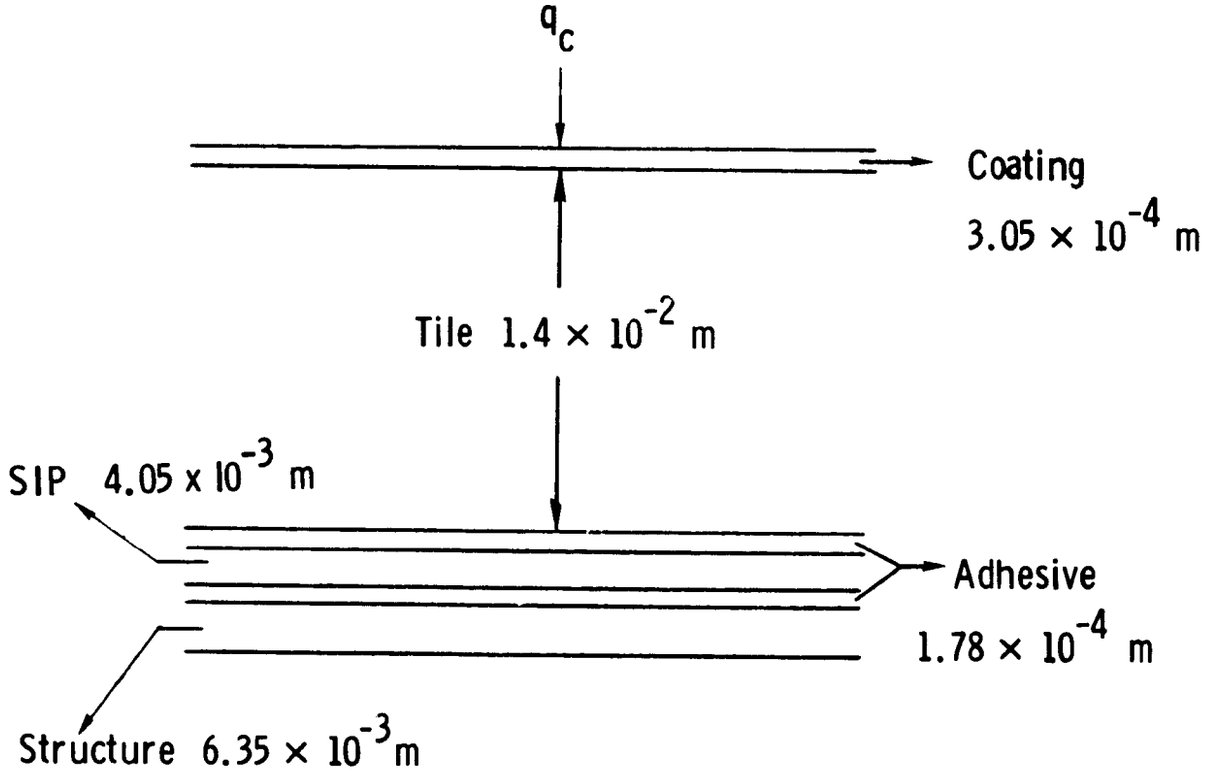

Figure 2.- LRSI thermal model (not drawn to scale).

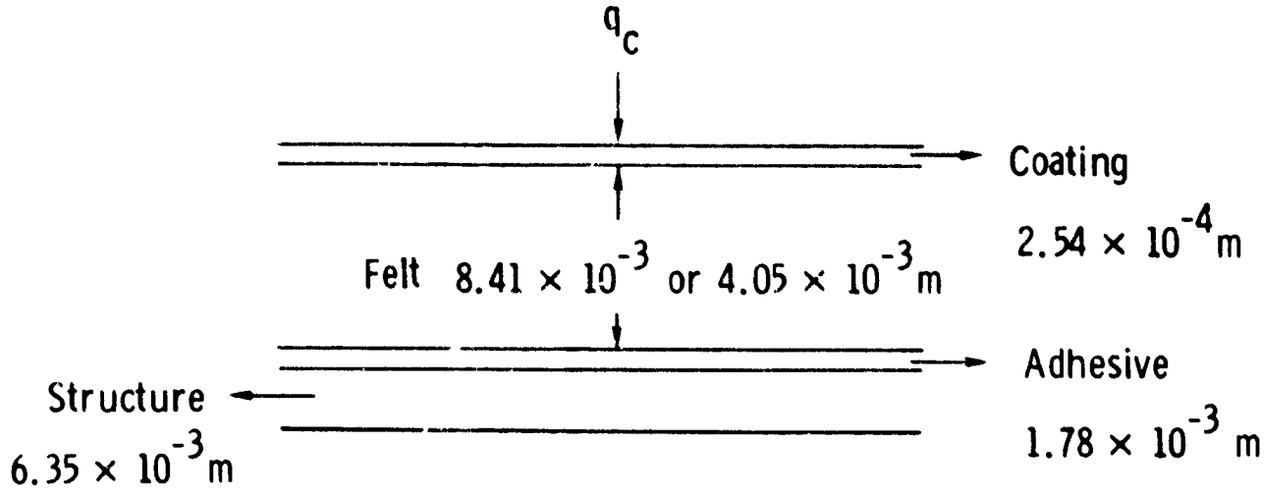

Figure 3.- FRSI thermal model (not drawn to scale).

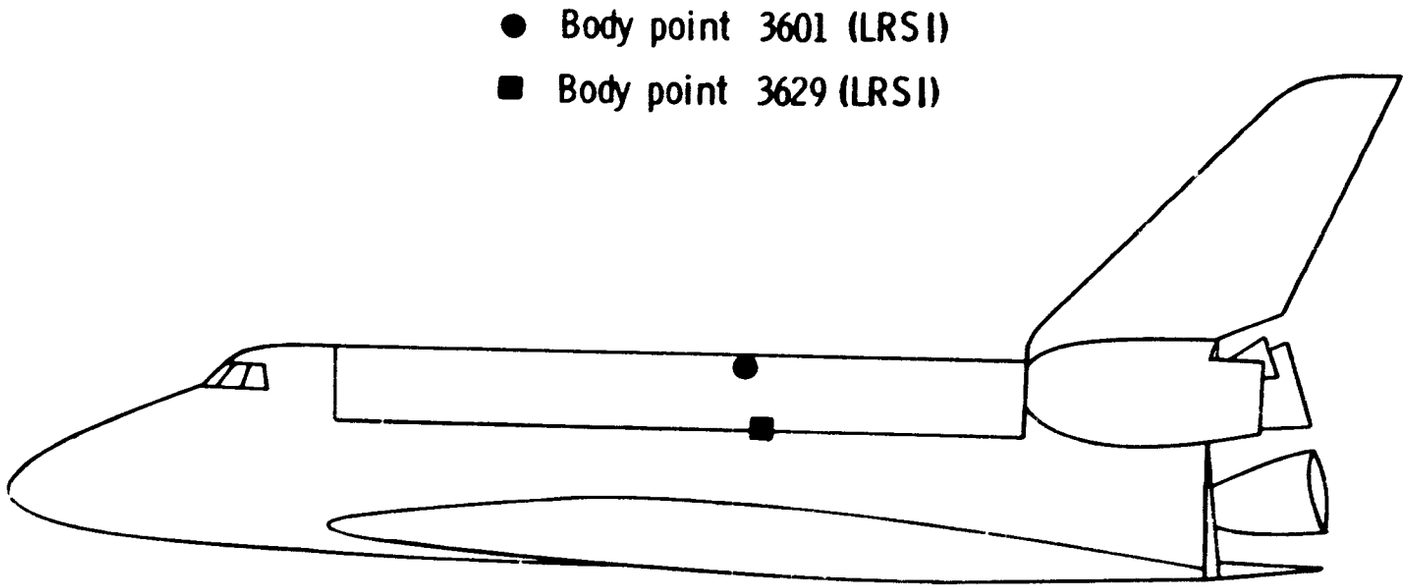

Figure 4.- Body point locations used. Side view.

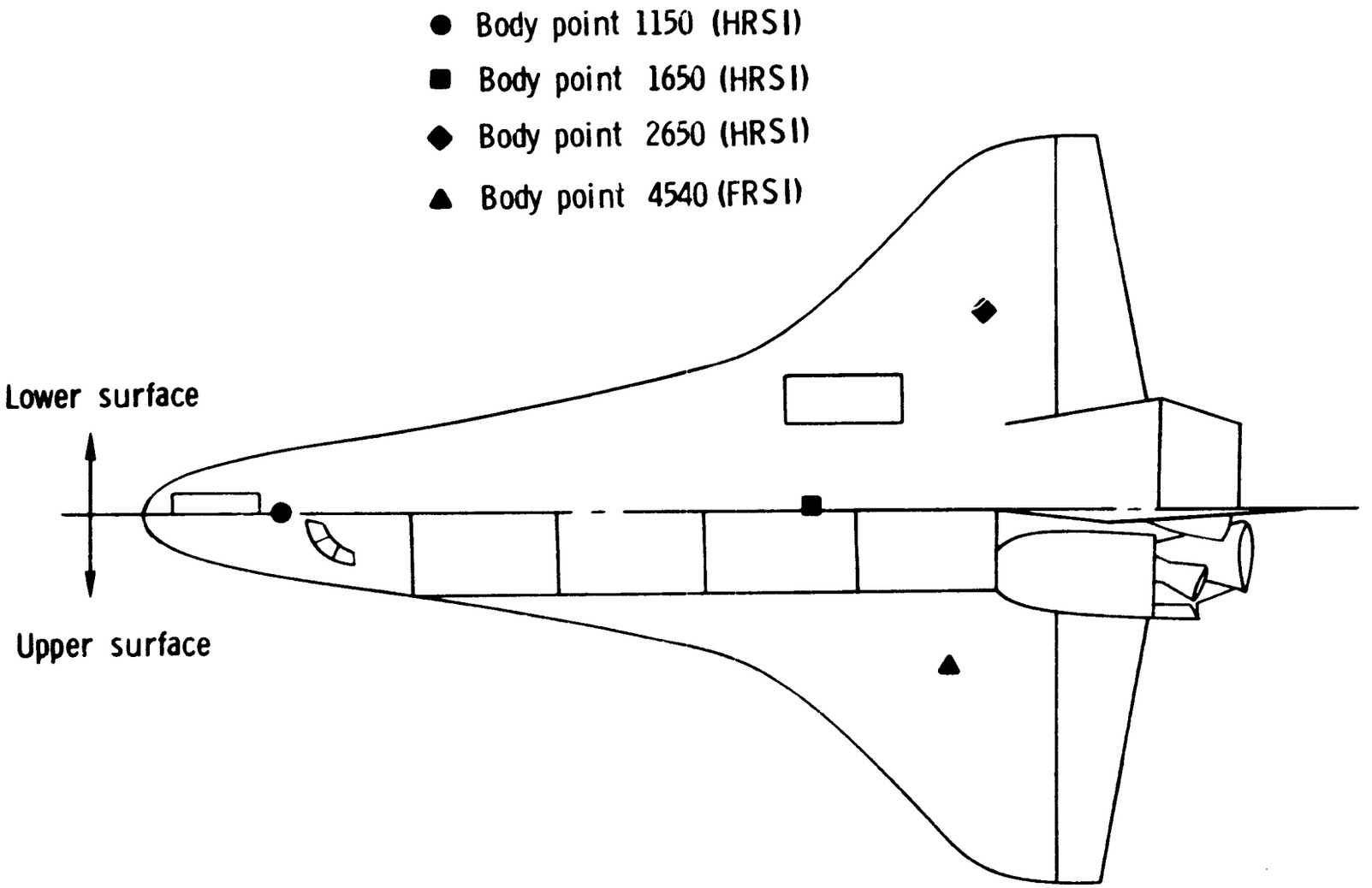

Figure 5.- Body point locations used. Upper lower view.

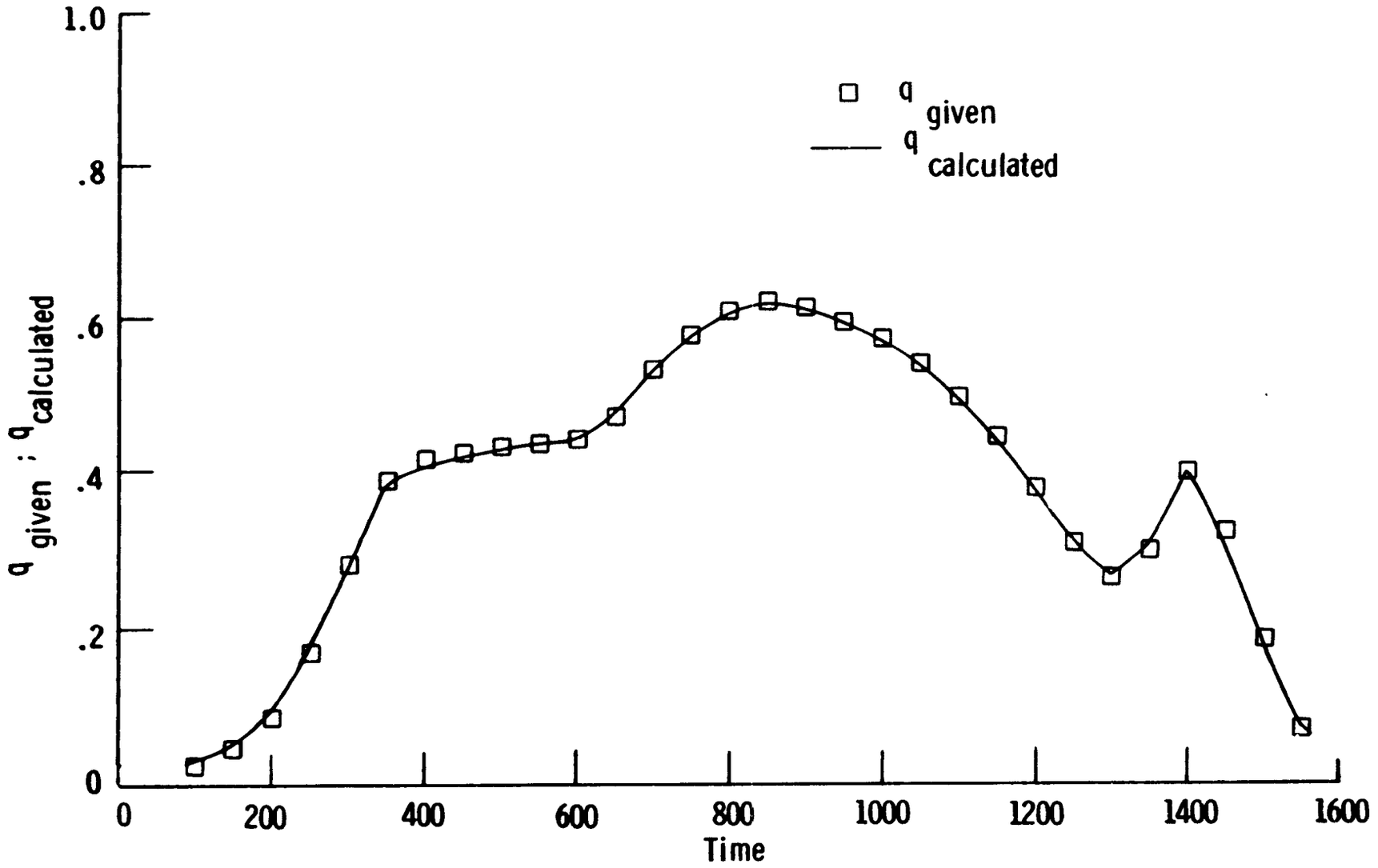

Figure 6.- Body point 3629, LRSI, comparison of direct (——) and inverse (□) methods.

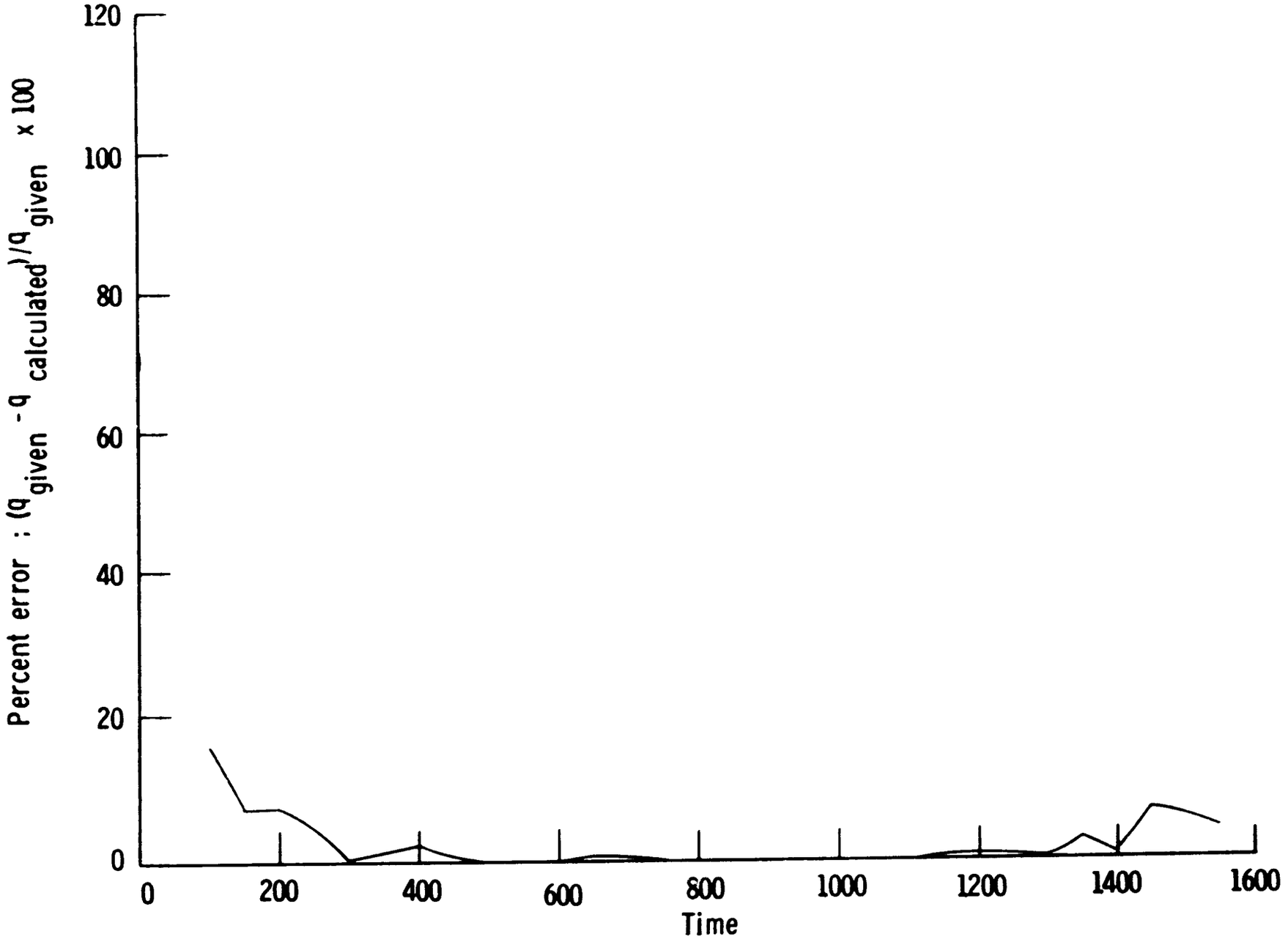

Figure 7.- Body point 3629, LRSI, error between direct and inverse methods.

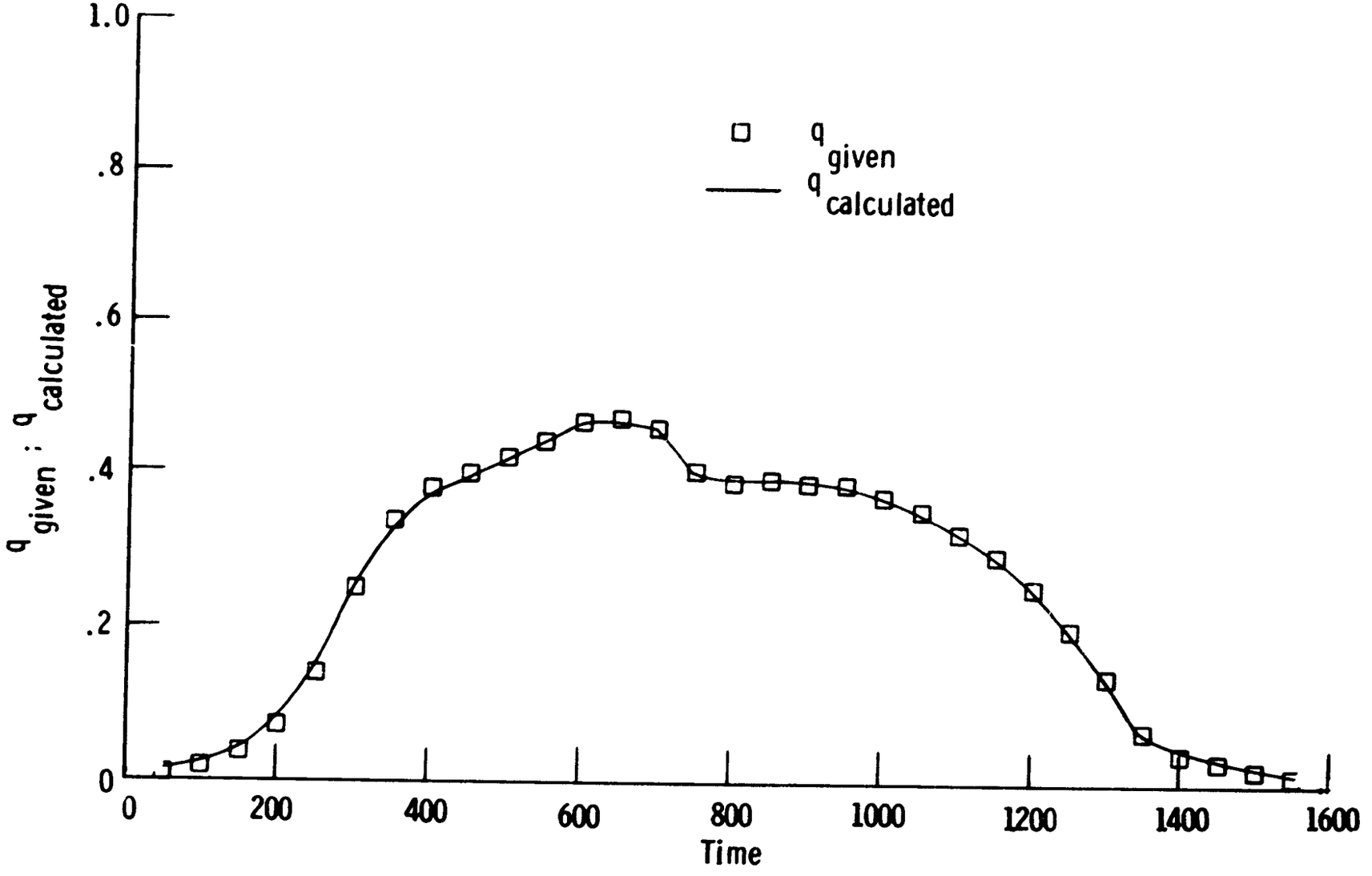

Figure 8.- Body point 3601, FRSI, comparison of direct (—) and inverse (□) methods.

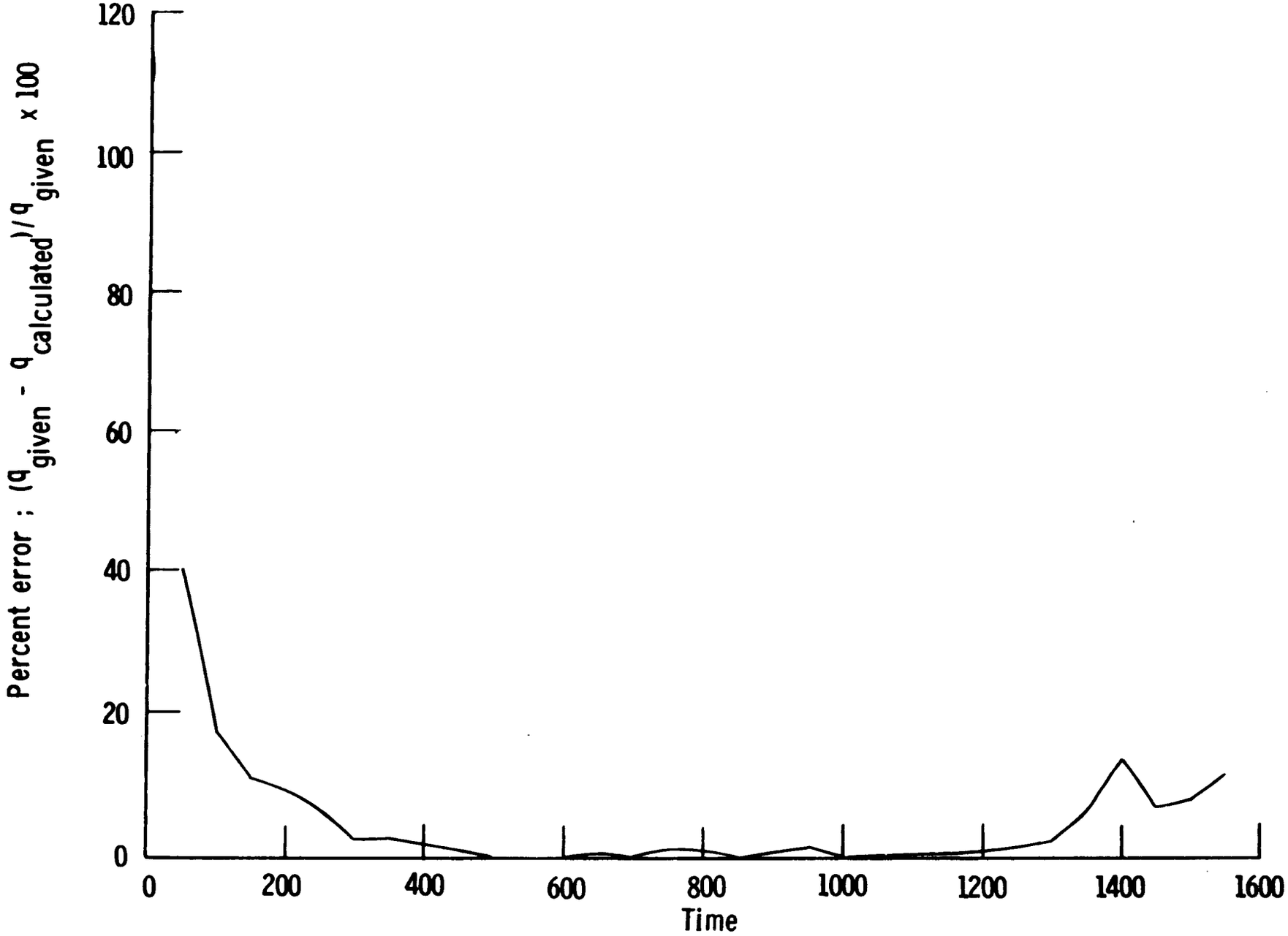

Figure 9.- Body point 3601, FRSI, error between direct and inverse methods.

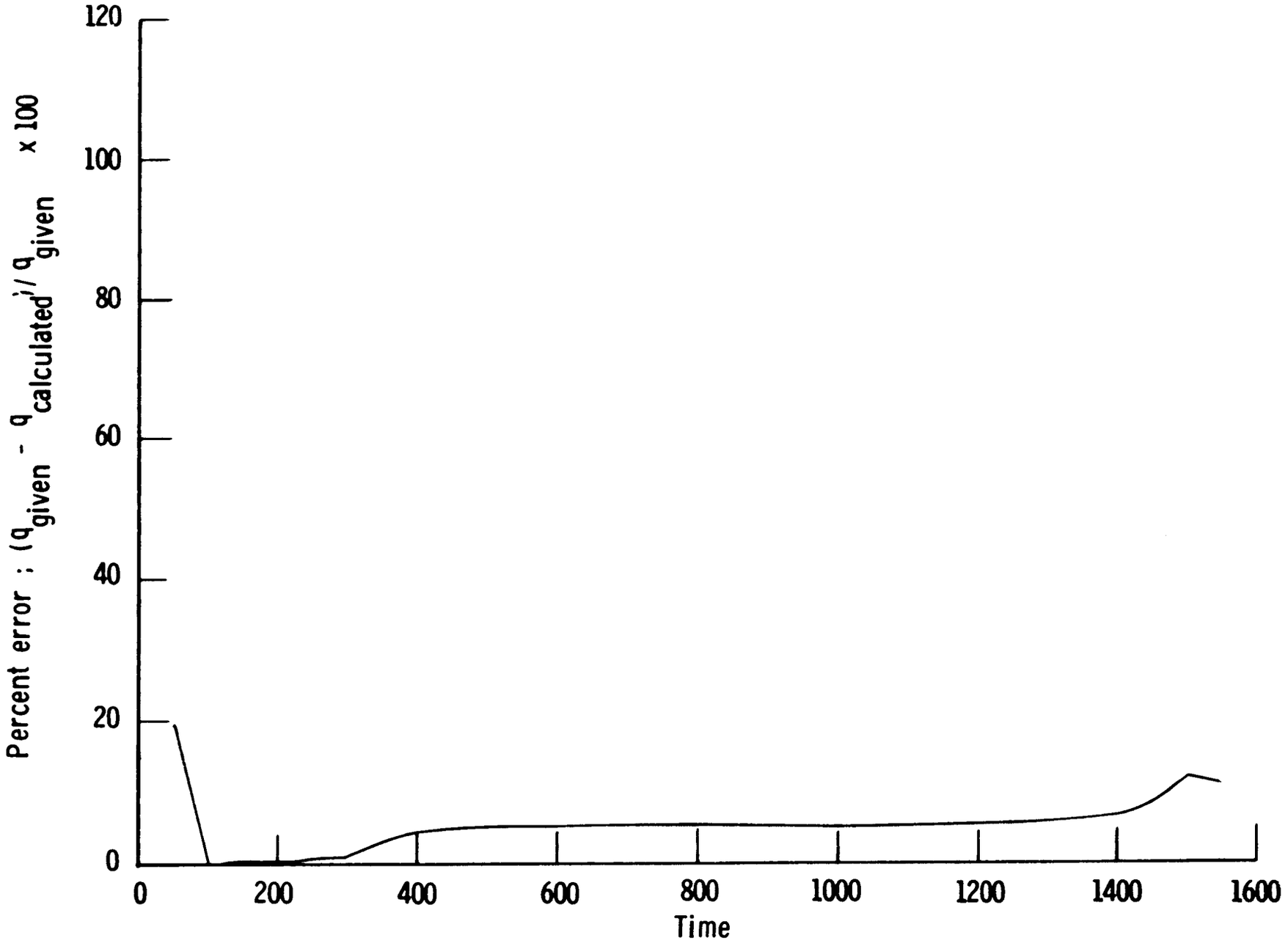

Figure 10.- Body point 2650, HRSI, 5 percent change in emittance, error between direct and inverse methods.

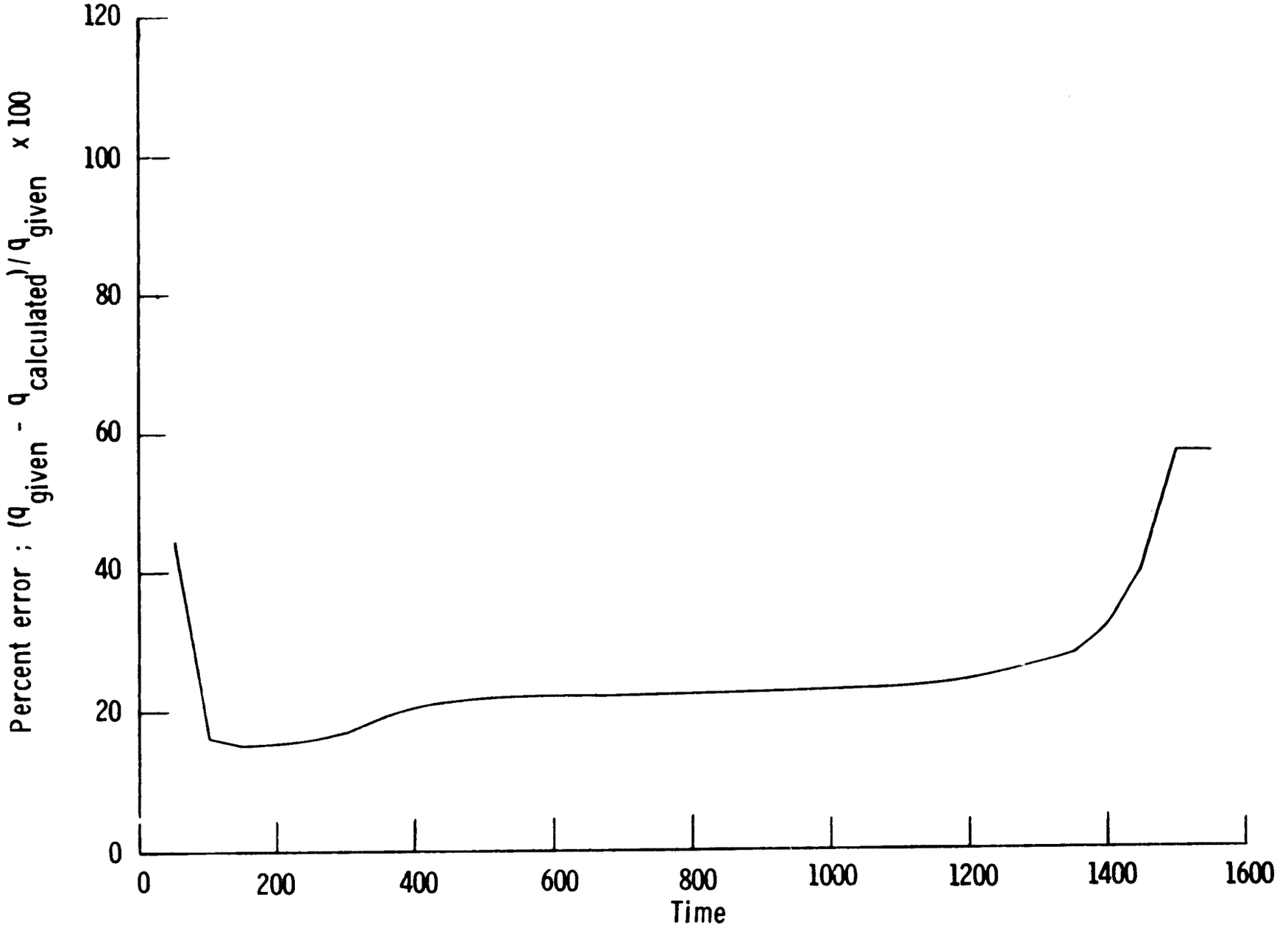

Figure 11.- Body point 1150, HRSI, 5 percent change in temperature, error between direct and inverse methods.

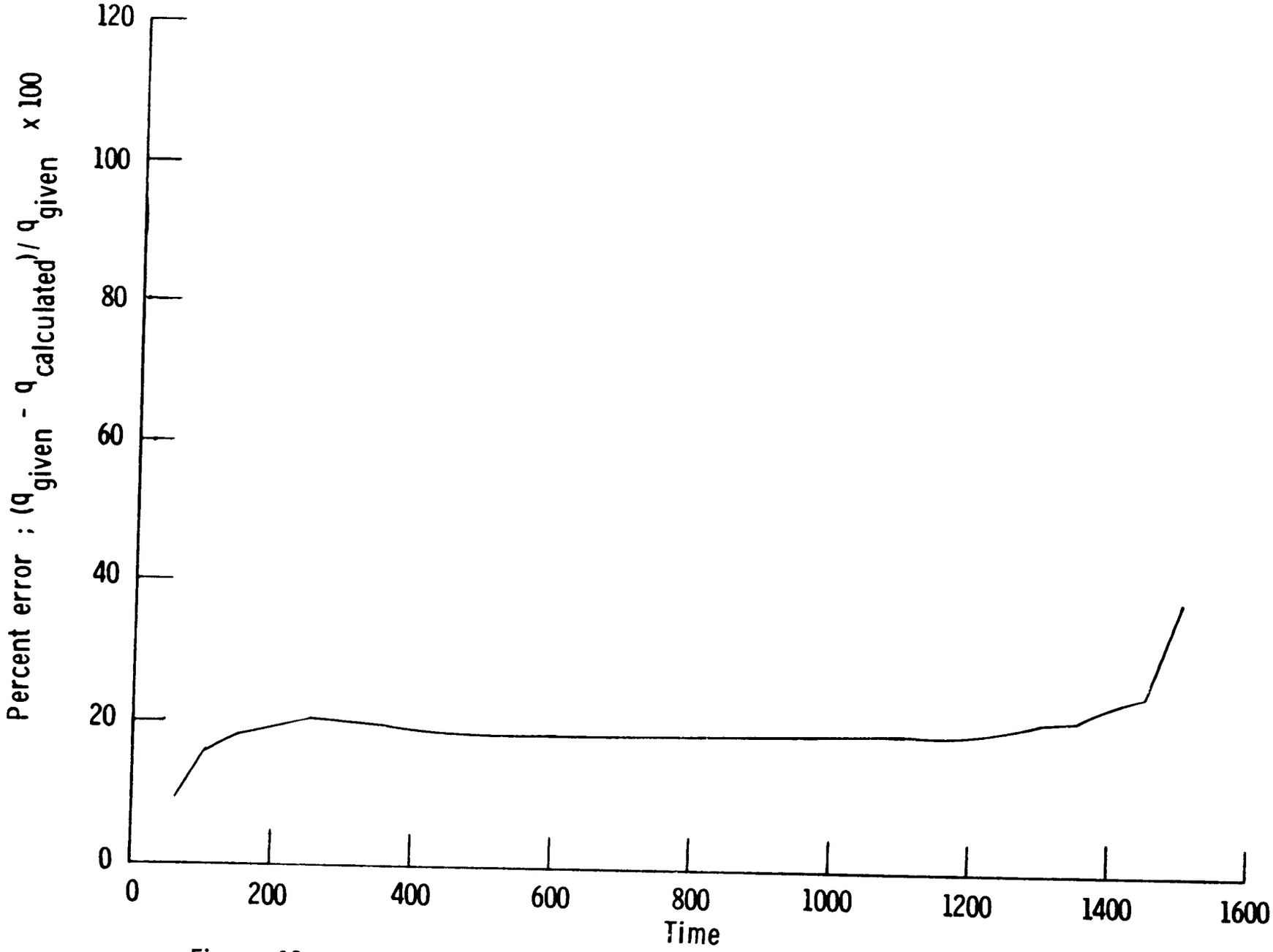

Figure 12.- Body point 1650, HRSI, -5 percent change in temperature, error between direct and inverse methods.

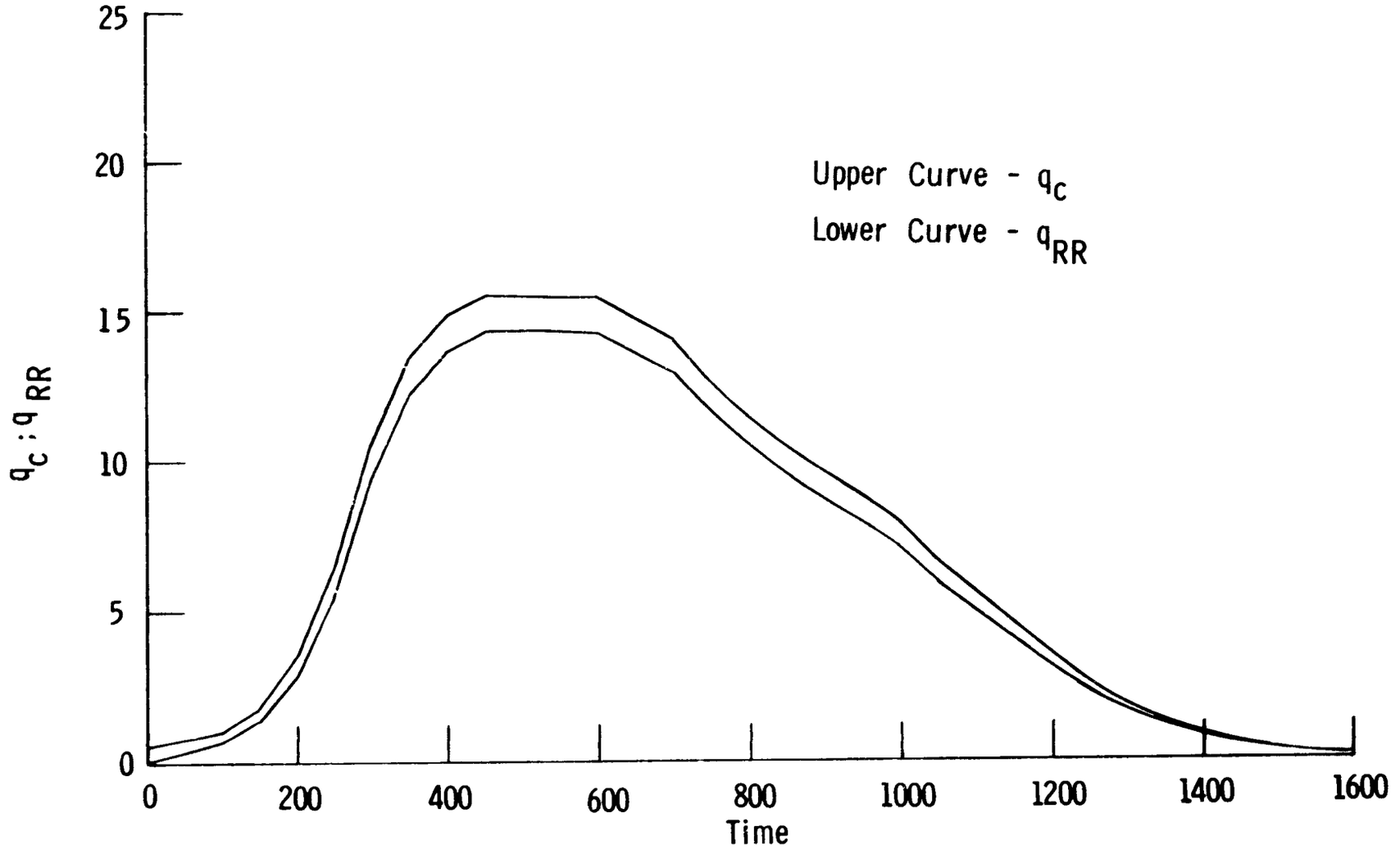

Figure 13.- Body point 1150, HRSI, plot of q_c and q_R showing influence of radiative term.

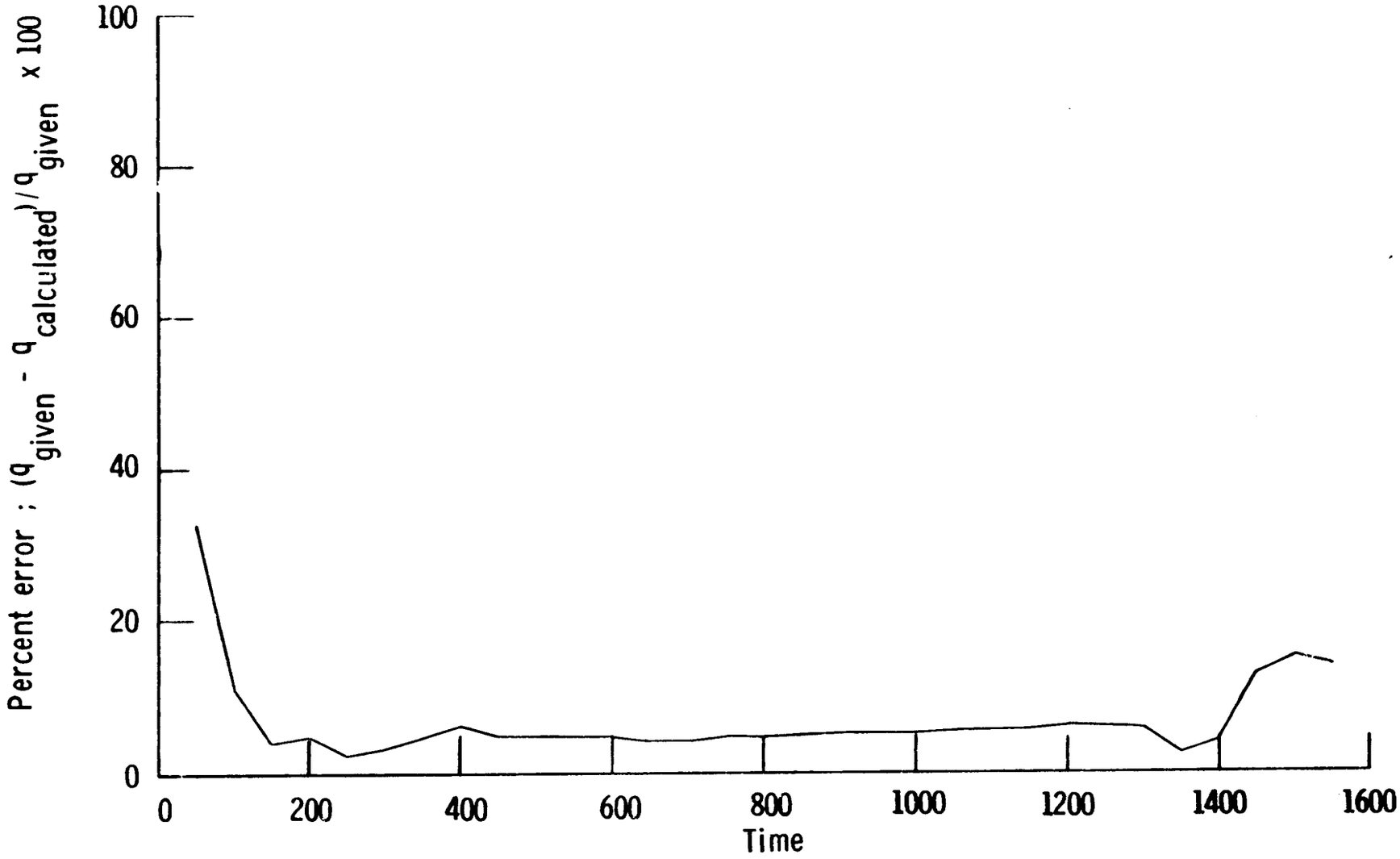

Figure 14.- Body point 3629, LRSI, 5 percent change in emittance, error between direct and inverse methods.

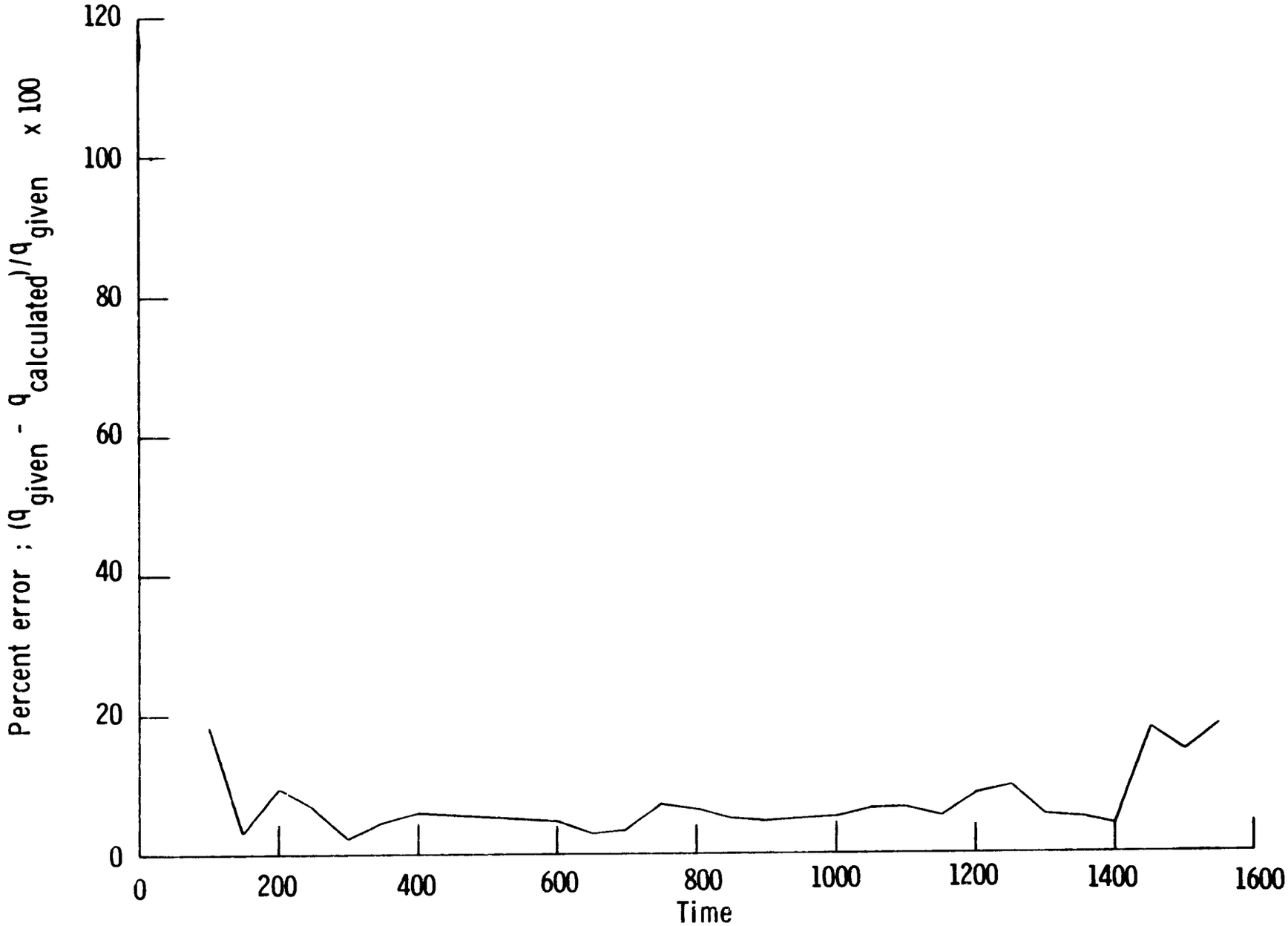

Figure 15.- Body point 4540, FRSI, 5 percent change in emittance, error between direct and inverse methods.

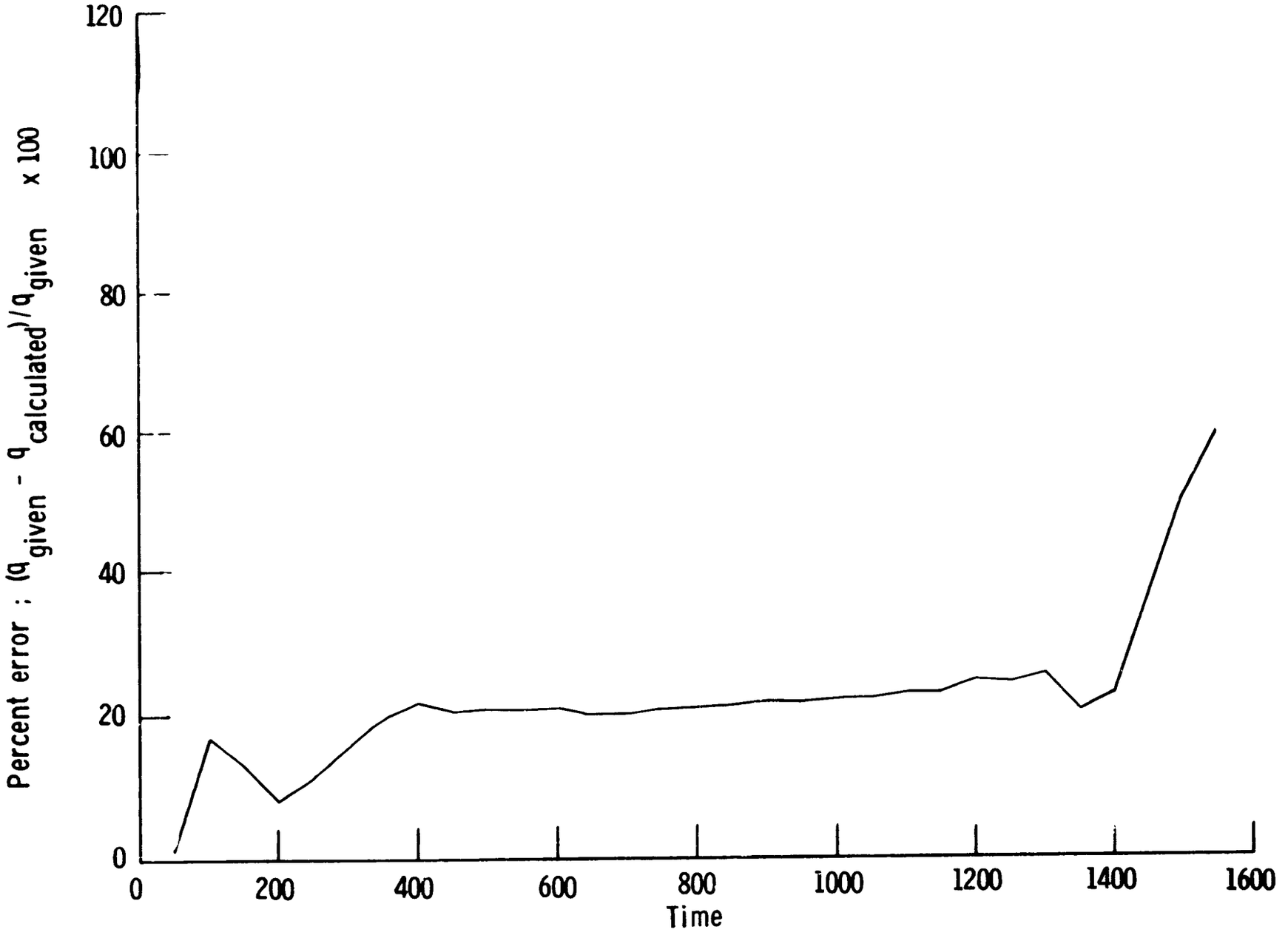

Figure 16.- Body point 3629, LRSI, 5 percent change in temperature, error between direct and inverse methods.

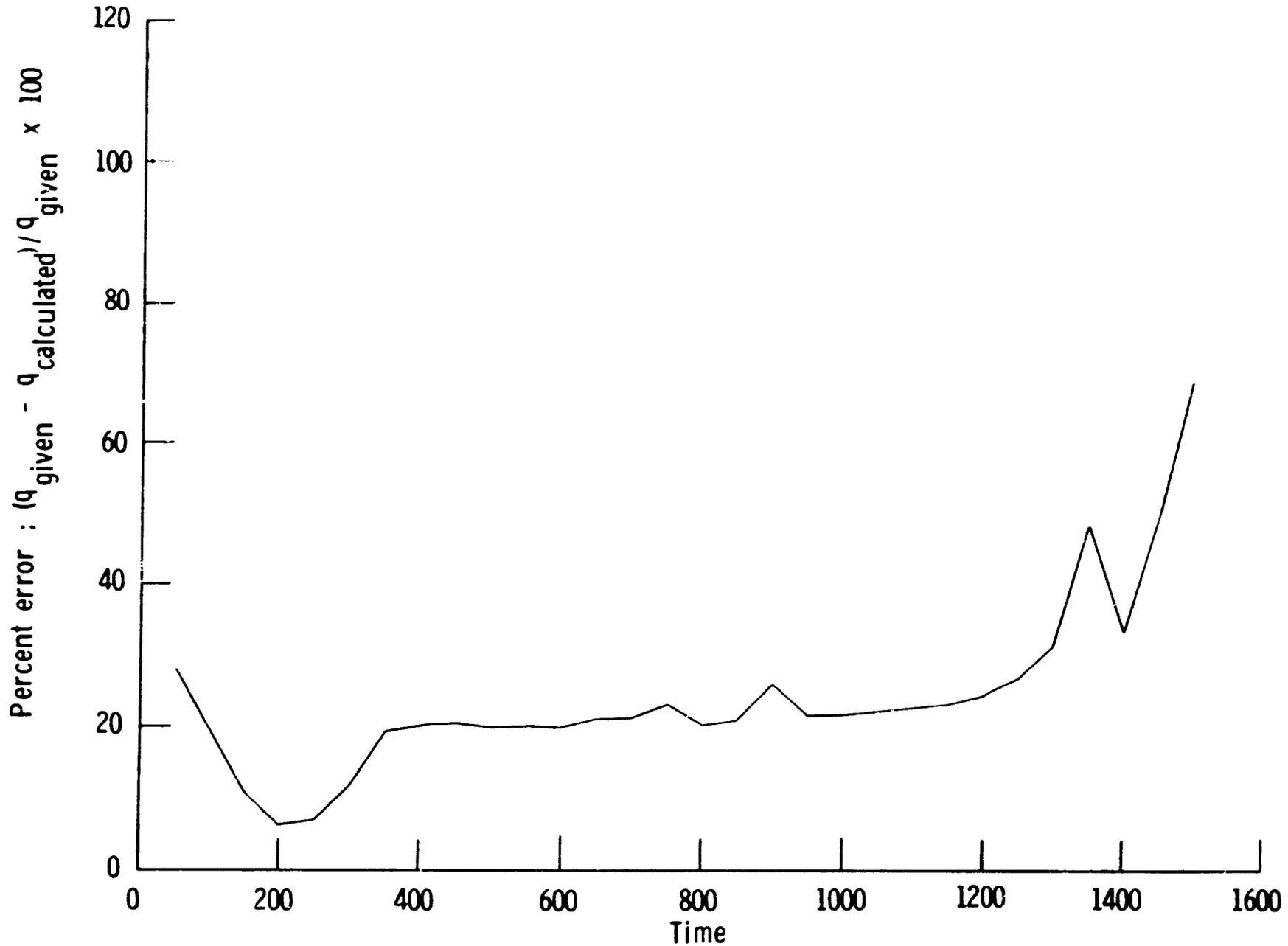

Figure 17.- Body point 3601, FRSI, 5 percent change in temperature, error between direct and inverse methods.

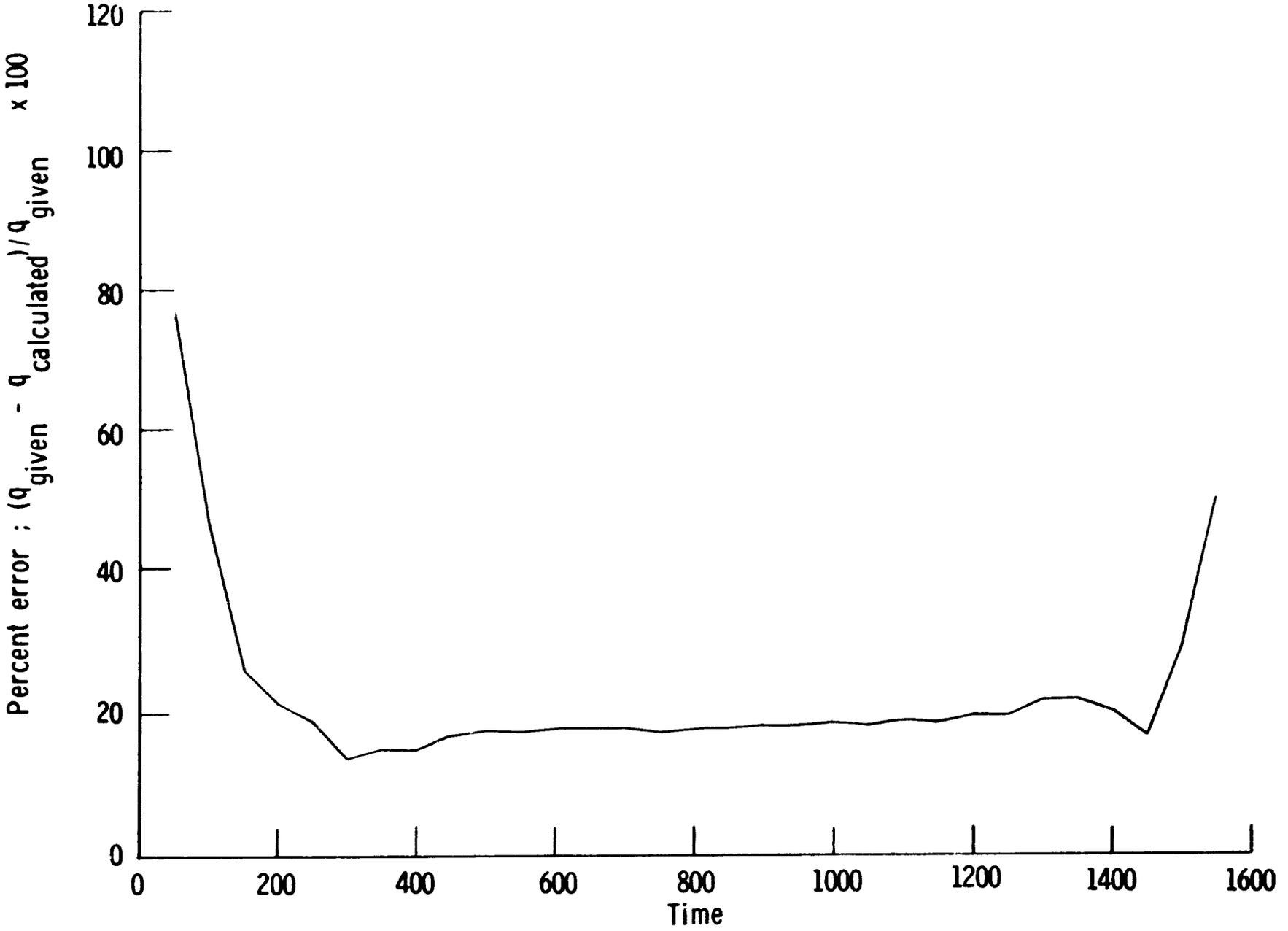

Figure 18.- Body point 3629, LRS1, -5 percent change in temperature, error between direct and inverse methods.

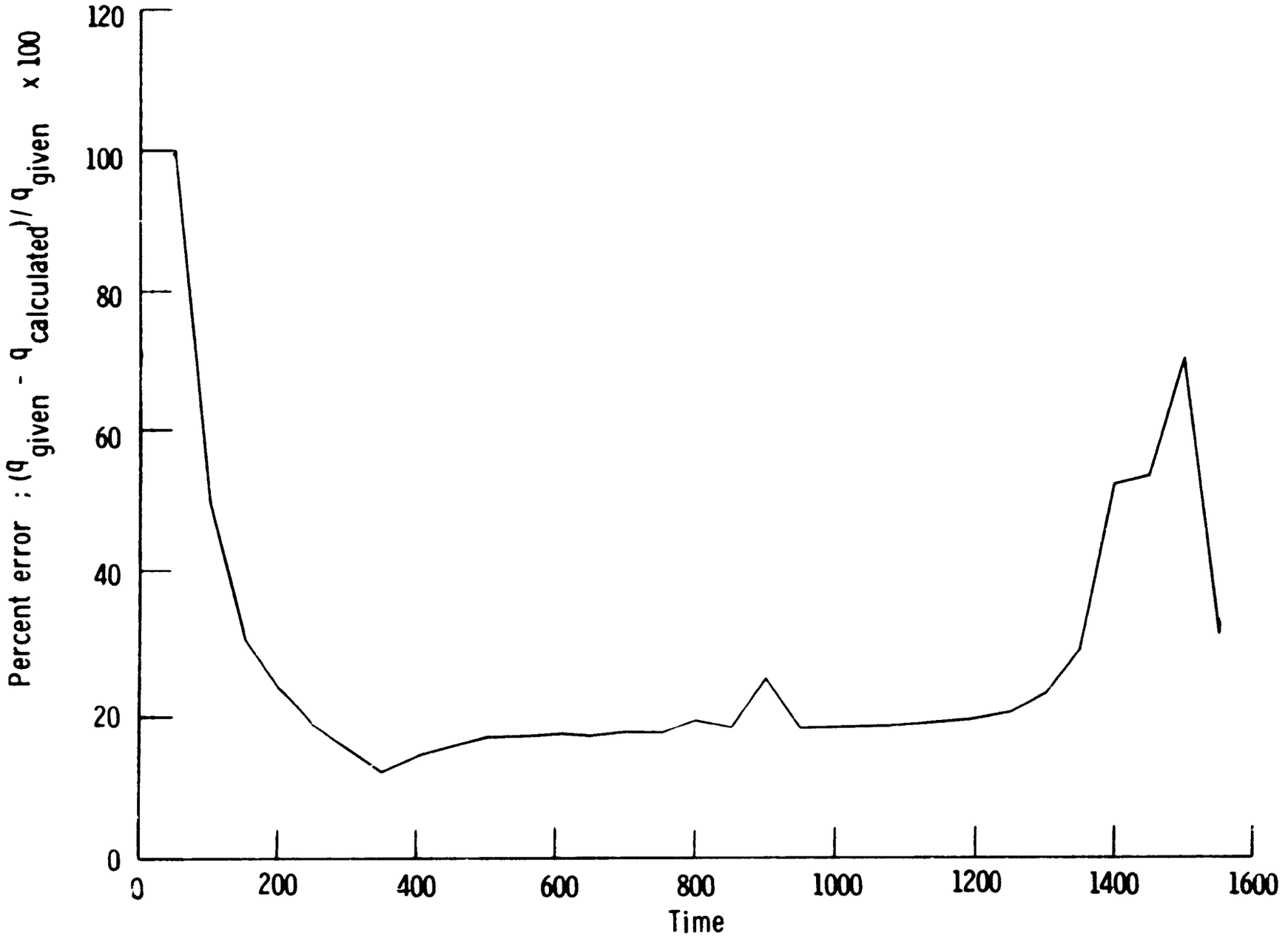

Figure 19.- Body point 3601, FRSI, -5 percent change in temperature, error between direct and inverse methods.

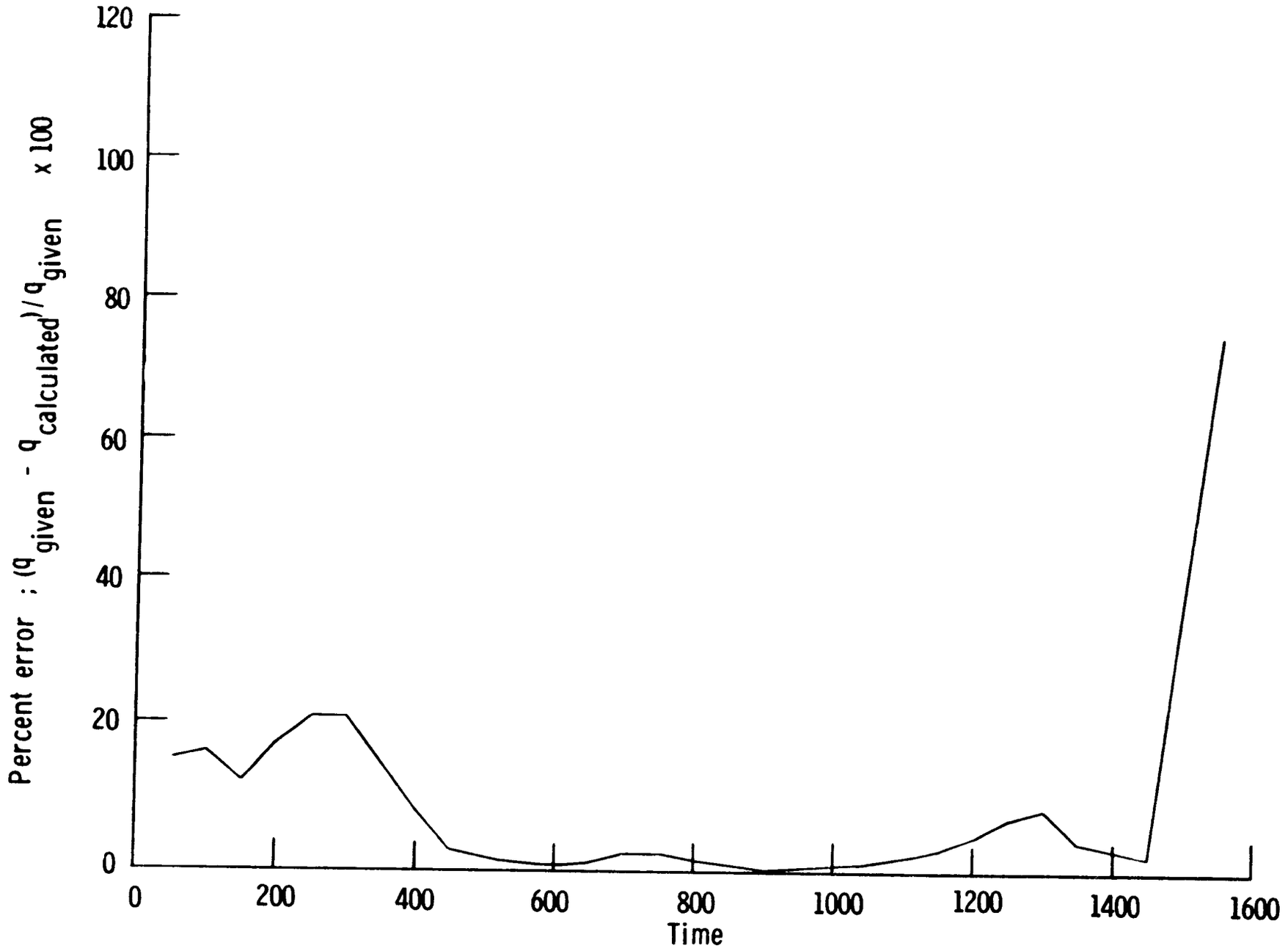

Figure 20.- Body point 3629, LRSI, 100 percent change in coating thickness, error between direct and inverse methods.

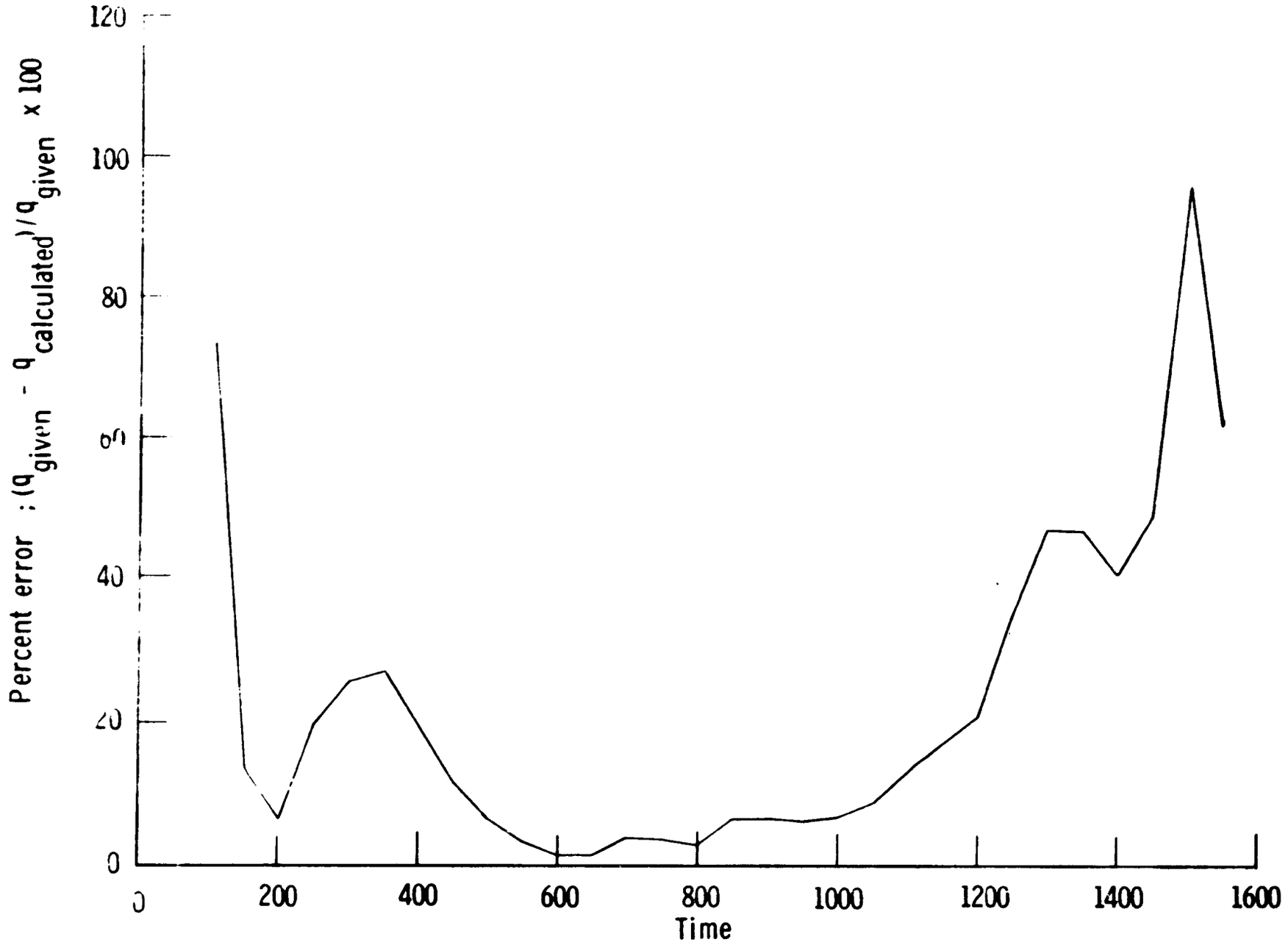

Figure 21.- Body point 4540, FRSI, 100 percent change in coating thickness, error between direct and inverse methods.

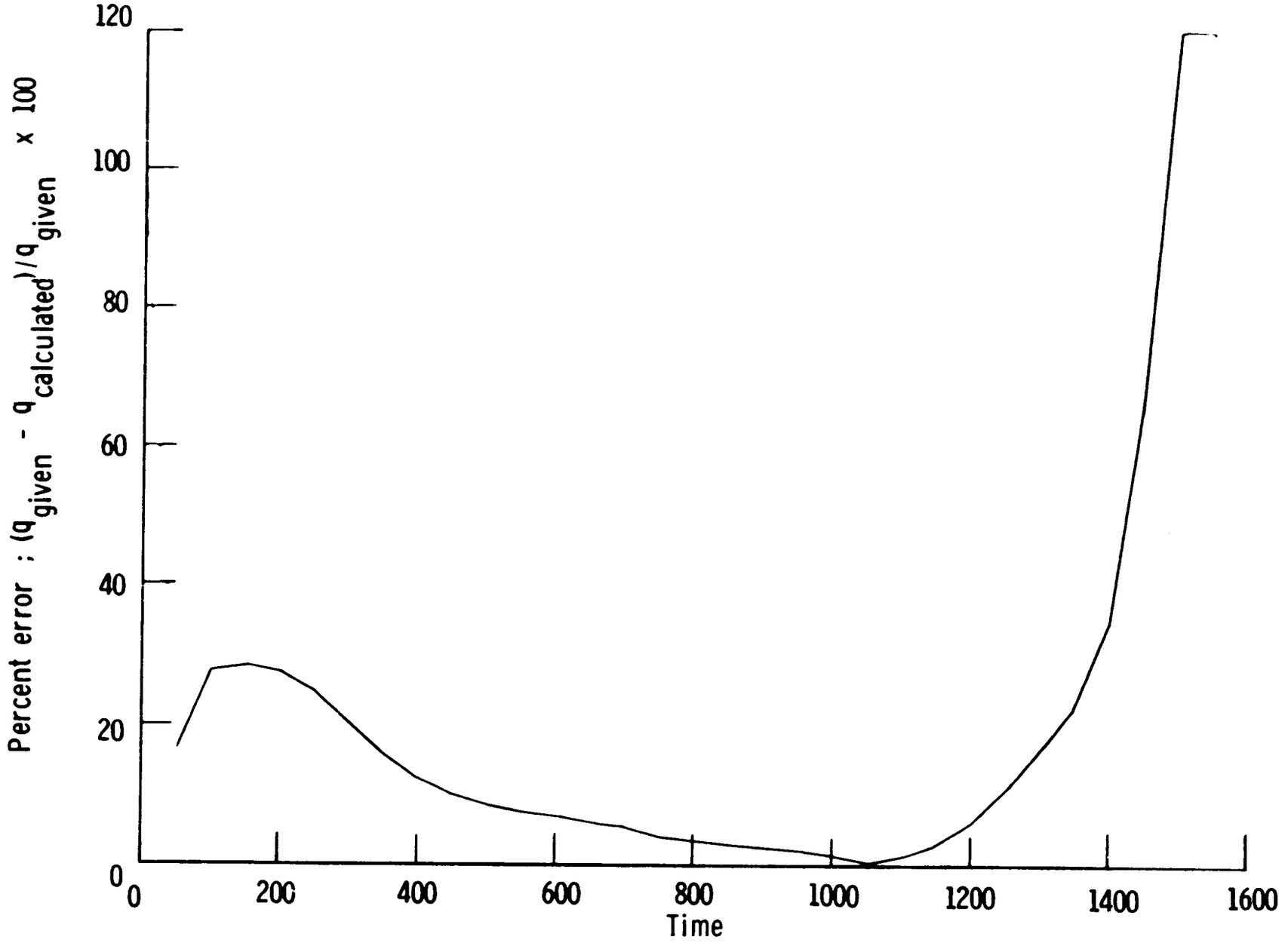

Figure 22.- Body point 1150, HRSI thermocouple depth error, error between direct and inverse methods.

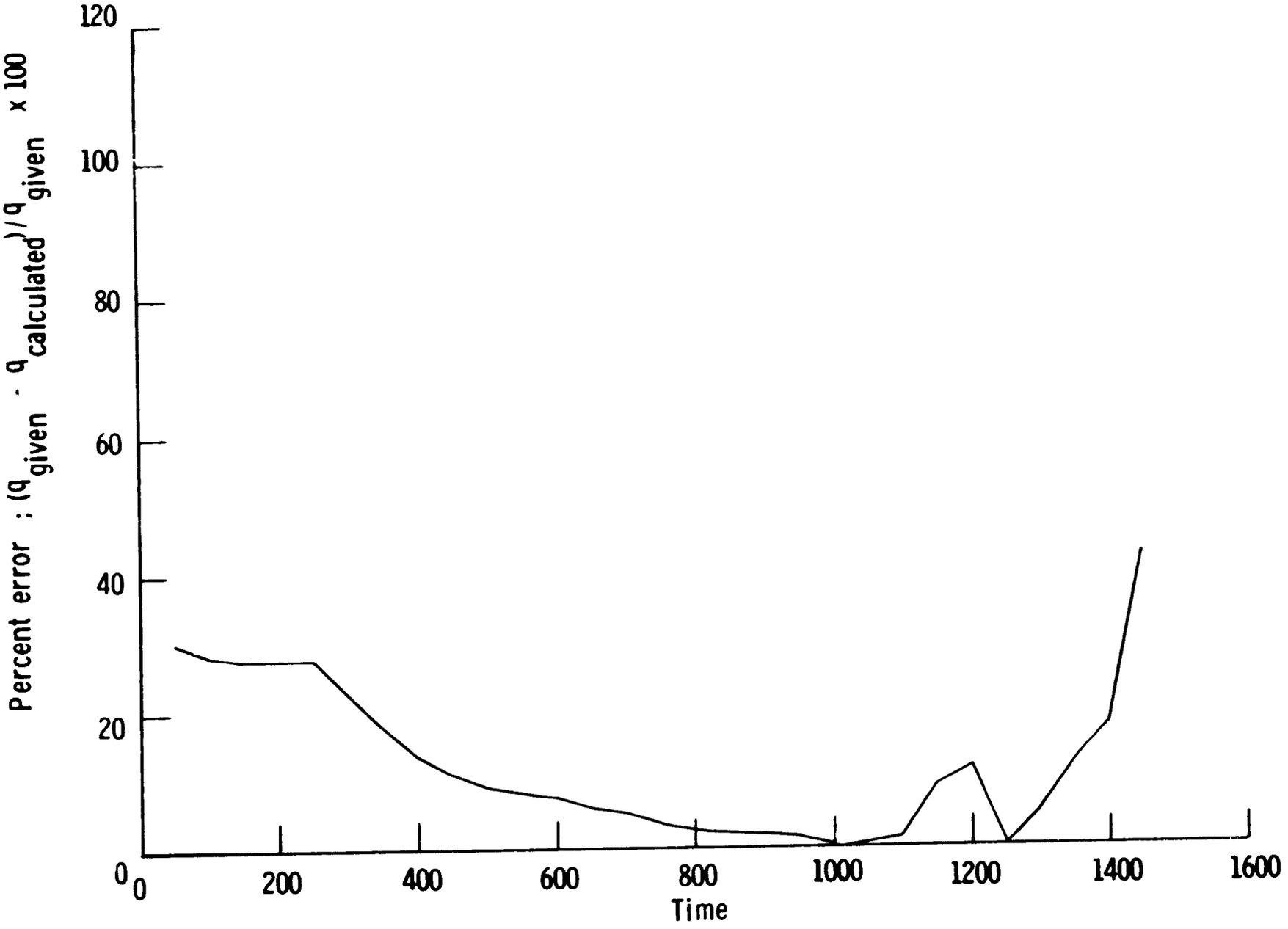

Figure 23.- Body point 1650, HRSI thermocouple depth error, error between direct and inverse methods.

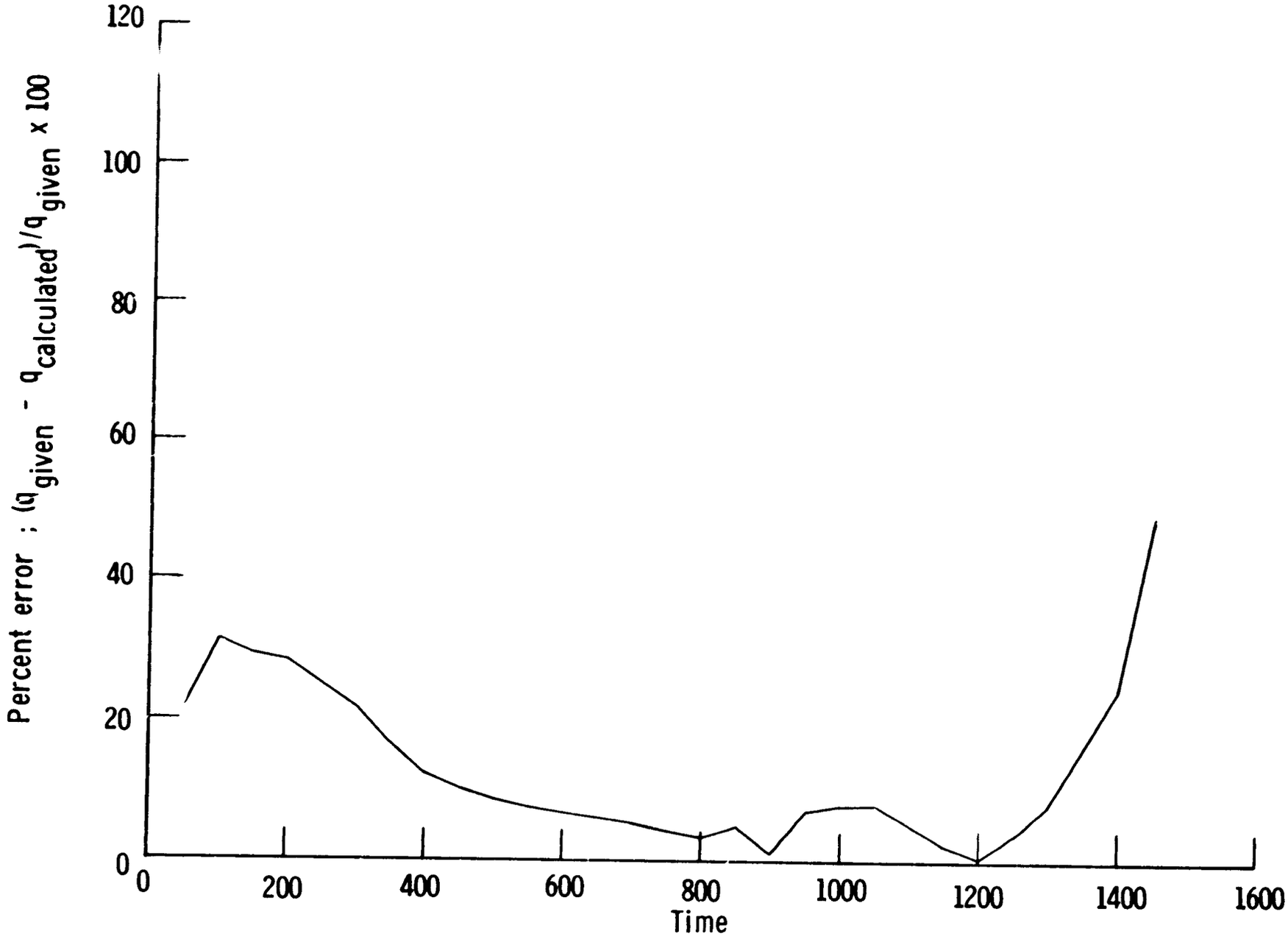

Figure 24.- Body point 2650, HRSI thermocouple depth error, error between direct and inverse methods.

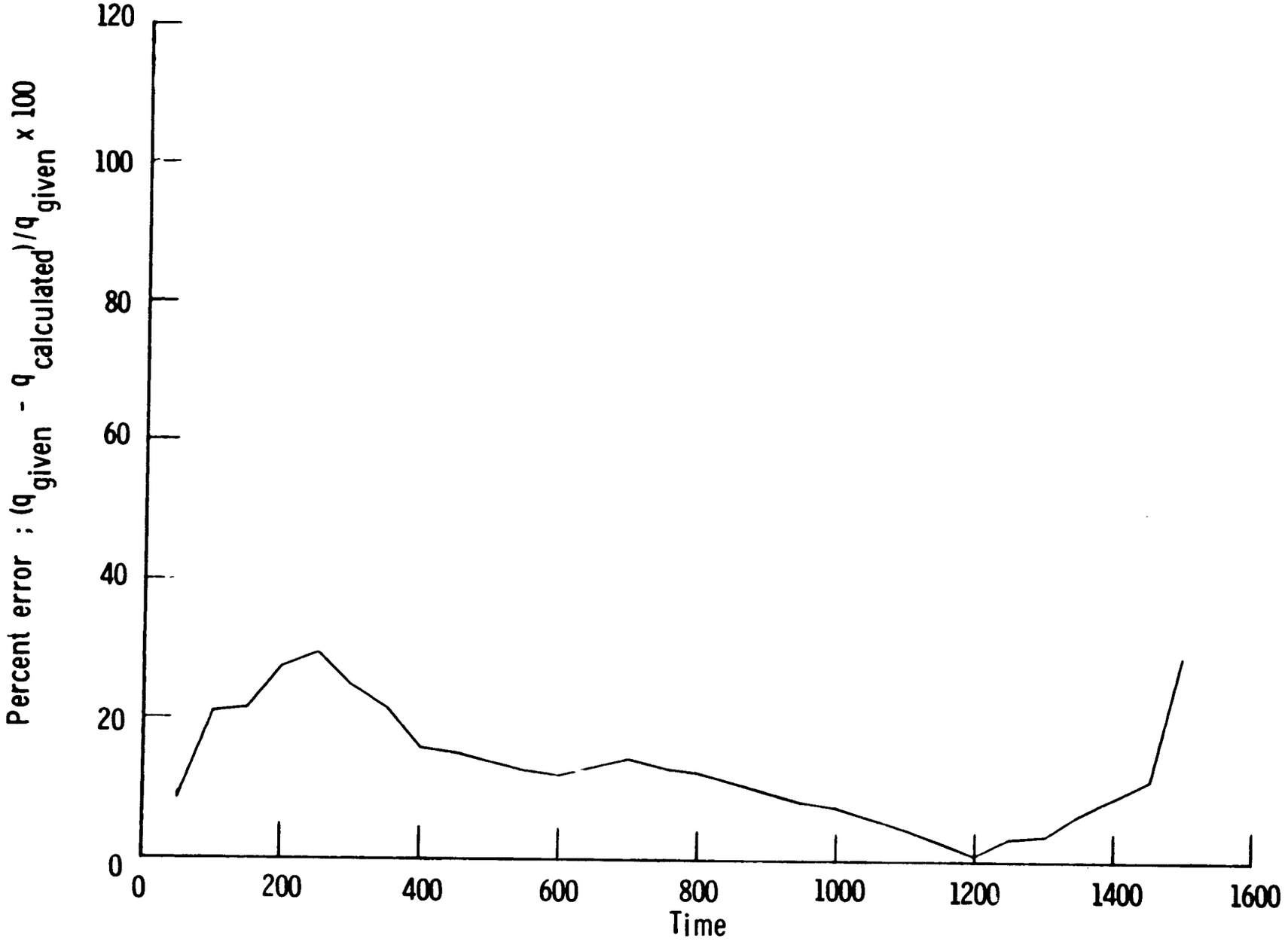

Figure 25.- Body point 3629, LRSI thermocouple depth error, error betwen direct and inverse methods.

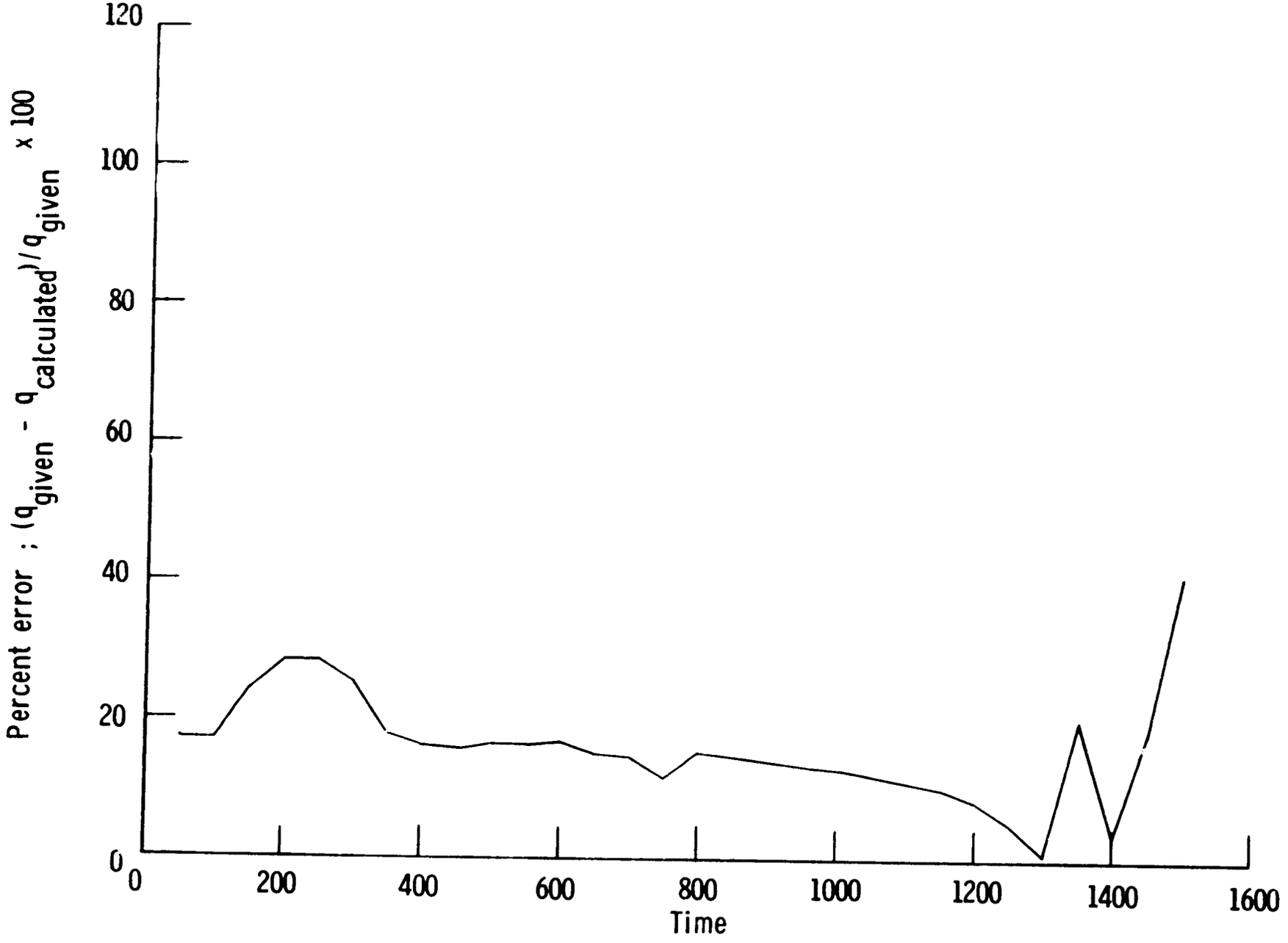

Figure 26.- Body point 3601, FRSI thermocouple depth error, error between direct and inverse methods.

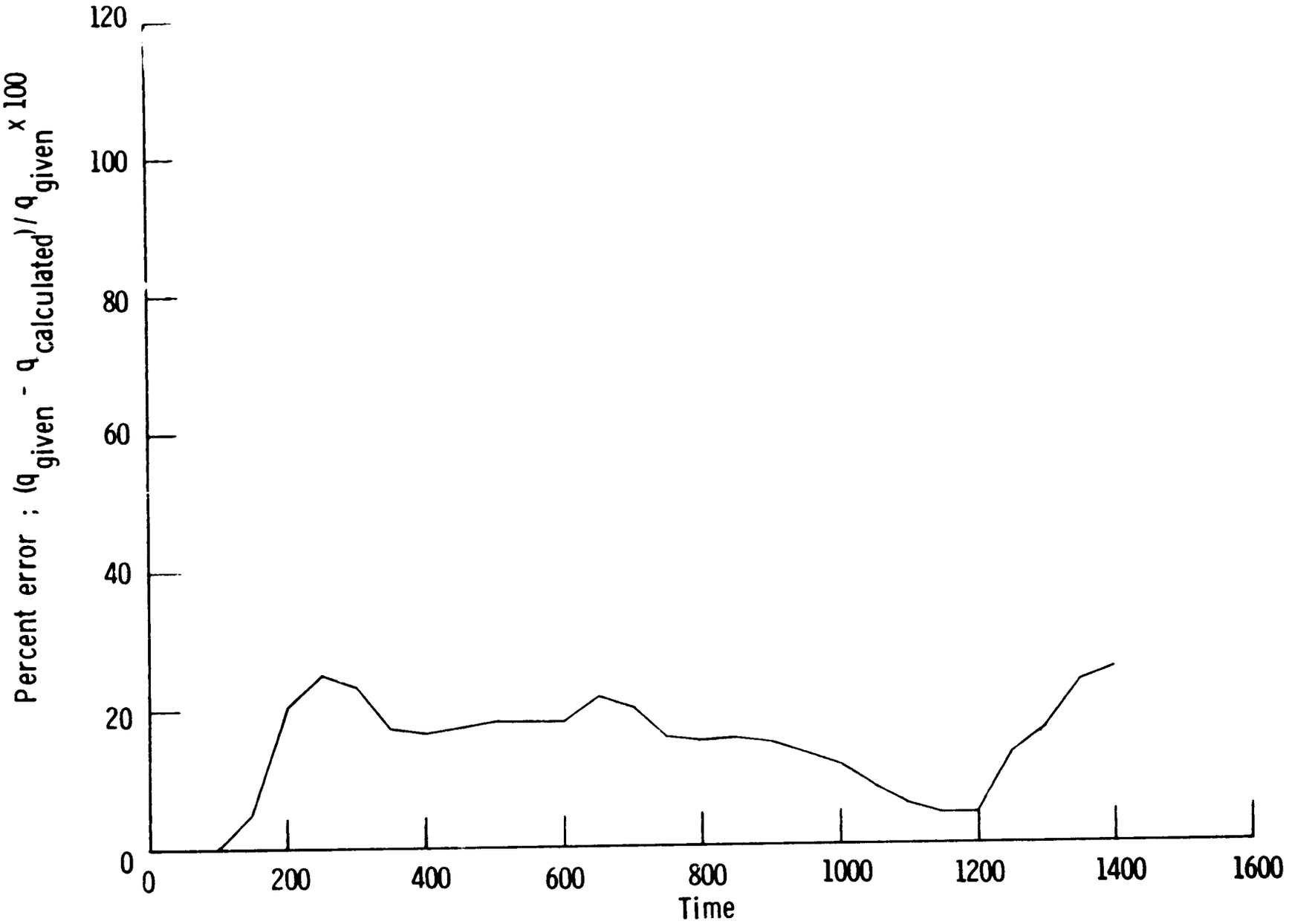

Figure 27.- Body point 4540, FRSI thermocouple depth error, error between direct and inverse methods.